$CD4^+$ T cells drive corneal nerve damage but are dispensable for corneal epitheliopathy development in dry eye disease

Authors: Alexia Vereertbrugghen[1], Manuela Pizzano[1], Agostina Cernutto[1], Florencia Sabbione[1], Irene A Keitelman[1], Douglas Vera Aguilar[1], Ariel Podhorzer[2], Federico Fuentes[3], Celia Corral-Vázquez[4], Mauricio Guzmán[4], Mirta N Giordano[1], Analía Trevani[1], Cintia S de Paiva[5], Jeremías G Galletti[1]

Affiliations:
1 Innate Immunity Laboratory, Institute of Experimental Medicine (CONICET/National Academy of Medicine of Buenos Aires), Buenos Aires, Argentina

2 Flow Cytometry Unit, Institute of Experimental Medicine (CONICET/National Academy of Medicine of Buenos Aires), Buenos Aires, Argentina

3 Confocal Microscopy Unit, Institute of Experimental Medicine (CONICET/National Academy of Medicine of Buenos Aires), Buenos Aires, Argentina

4 Translational Clinical Research Program, Hospital del Mar Research Institute, Barcelona, Spain

5 Ocular Surface Center, Baylor College of Medicine, Houston, Texas, USA

All authors declare that there is no conflict of interest.

Keywords: corneal nerves, neuropathy, CD4 T cells, autoimmunity, immunopathology

Abstract

Dry eye disease (DED) is a disorder characterized by a dysfunctional tear film in which the corneal epithelium and its abundant nerves are affected by ocular desiccation, inflammation, and the local immune response. Although adaptive immunity and specifically $CD4^+$ T cells play a role in DED pathogenesis, the exact contribution of these cells to corneal epithelial and neural damage remains undetermined. To address this, we explored the progression of a surgical DED model in wild-type (WT) and T cell-deficient mice. We observed that adaptive immune-deficient mice developed all aspects of DED comparably to WT mice except for the absence of functional and morphological corneal nerve changes, nerve damage-associated transcriptomic signature in the trigeminal ganglia, and sustained tear cytokine levels. Adoptive transfer of $CD4^+$ T cells from DED WT mice to T cell-deficient mice reproduced corneal nerve damage but not epitheliopathy. Conversely, T cell-deficient mice reconstituted solely with naive $CD4^+$ T cells developed corneal nerve impairment and epitheliopathy upon DED induction, thus replicating the WT DED phenotype. Collectively, our data show that while corneal neuropathy is driven by $CD4^+$ T cells in DED, corneal epithelial damage develops independently of the adaptive immune response. These findings have implications for T cell-targeting therapies currently in use for DED.

1. Introduction

The ocular surface is the mucosal microenvironment that encircles the cornea and keeps it moist and protected for proper sight(1,2). Ocular surface homeostasis depends on a delicate balance between all of its components: the cornea, the conjunctiva, the tear film, the eyelids, the lacrimal and meibomian glands, the ocular surface immune system, and ocular surface innervation. Dry eye disease (DED) is an increasingly prevalent ocular surface disorder characterized by a dysfunctional tear film, visual disturbance, local inflammation and tissue damage, neurosensory abnormalities, and symptoms ranging from ocular discomfort to overt pain(3). The diverse components of the ocular surface are varyingly affected in DED, leading to heterogeneous clinical presentations. While some patients have overt ocular surface epitheliopathy accompanied by discomfort or pain, others present mainly with symptoms derived from neurosensory alterations and little or no ocular epithelial damage(4,5). Within the multifactorial pathophysiology of DED, ocular surface inflammation plays a pivotal role in perpetuating the disease by favoring tissue damage, which in turn elicits more inflammation and creates a vicious cycle(6–8). However, if differences in the ocular surface inflammatory and immune responses lead to the DED clinical spectrum is unclear.

A large body of evidence indicates that $CD4^+$ T cells become key drivers of DED-associated ocular inflammation by orchestrating the local adaptive immune response(7,8). Clinical studies show that DED patients have higher numbers of conjunctival $CD4^+$ T cells(9) and at least two FDA-approved drugs (cyclosporine and lifitegrast) for topical anti-inflammatory therapy selectively block T cell activation in the ocular surface(7,10). In animal models, the adoptive transfer of $CD4^+$ T cells from DED mice into T cell-deficient recipients reproduces the conjunctival goblet cell loss and lacrimal gland infiltration observed in donor mice(11,12) while depletion of ocular surface antigen-presenting cells prevents local $CD4^+$ T cell activation and goblet cell loss(13). Moreover, DED increases the number of T-helper (Th)1 and Th17 $CD4^+$ T cells in the eye-draining lymph nodes(14,15) of mice, and consistently, both interferon (IFN)-γ and interleukin (IL)-17 are increased in the tears and conjunctiva of DED patients(16–19). Dysfunctional regulatory $CD4^+$ T cells also contribute to DED pathogenesis by not restraining effector $CD4^+$ T cells(20–22).

Effector $CD4^+$ T cells in DED are mostly Th1 and Th17(14,15), which promote type 1 and type 3 immunity, respectively(23), by releasing proinflammatory cytokines and recruiting other immune cells(23,24). IFN-γ, a hallmark type 1 cytokine, exerts a deleterious effect on the ocular surface by promoting both the apoptosis of conjunctival goblet cells and corneal epithelial cells and the squamous metaplasia of corneal epithelial cells(12,25–29). IL-17, a hallmark type 3 cytokine, induces corneal epithelial cells to secrete matrix metalloproteinases, which degrade intercellular junctions and lead to corneal barrier disruption(19,30). IL-17 also favors corneal lymphangiogenesis, which facilitates the migration of corneal antigen-presenting cells and, thus, pathogenic immune responses(31). IFN-γ and IL-17 have additional effects on corneal and conjunctival epithelial, stromal, and immune cells that amplify ocular surface inflammation and

tissue damage(29). However, it should be noted that $CD4^+$ T cells are not the only source of the pathogenic IFN-γ and IL-17 in the ocular surface because $CD8^+$ T cells, γδ T cells, NK cells, and other innate lymphoid cells also secrete these cytokines(32,33). In the setting of DED, NK cells contribute early to IFN-γ levels while γδ T cells also produce IL-17(34–37). Thus, while the pathogenicity of type 1 and 3 immunity in DED-associated corneal epitheliopathy is firmly established, it may be mediated by $CD4^+$ T cells and innate immune cells(35).

Contrasting the ample evidence on the pathogenic mechanisms that lead to ocular surface epitheliopathy, the pathophysiology of neurosensory abnormalities in DED has not been explored in such detail(38,39). The intraepithelial endings of the corneal nerves are almost in direct contact with the tear film and are the most impacted corneal nerve segments in DED. Since these nerves rely entirely on corneal epithelial cells for support(40), become affected early in the course of the disease(41), and their impairment coincides with corneal epitheliopathy development, it is assumed that corneal nerve damage in DED is secondary to corneal epitheliopathy and caused by the same mechanisms. However, the heterogeneous presentations of DED include a neuropathic form with minimal corneal epitheliopathy and ocular surface inflammation but overt symptoms and detectable corneal nerve alterations(5). In line with this, we observed in a murine tear hyperosmolarity model that corneal nerve changes can ensue in the absence of corneal barrier disruption(42), and more recently, that corneal neuropathy may develop independently of corneal epitheliopathy if a type 1 immune response is present in the ocular surface(43). However, since both models lack ocular desiccation, the defining disease feature that initiates corneal pathology(3,4), their conclusions may not apply to DED because additional mechanisms could be at play. The disease setting determines the pathogenic impact (or lack thereof) of the local immune response on the corneal nerves: herpetic keratitis and ocular graft-versus-host-disease but not ocular allergy exhibit corneal neuropathy despite all three being immune-driven ocular surface disorders(44). In the case of DED, whether local $CD4^+$ T cell-coordinated adaptive immunity in the context of ocular desiccation contributes to corneal neuropathy has not been fully explored.

We hypothesized that the $CD4^+$ T cell-coordinated adaptive immune response in DED may induce corneal neuropathy independently from corneal epitheliopathy. Therefore, we set out to explore the relative contribution of the adaptive immune response, and more specifically of $CD4^+$ T cells, to corneal epithelial and nerve damage in a murine model of DED.

2. Materials and methods

2.1 Mice

C57BL/6 (C57BL/6NCrl) mice were originally obtained from Charles River Laboratories (Wilmington, MA, USA) and recombination-activating gene 1 (*Rag1*)-knockout (*Rag1*KO (B6.129S7-Rag1tm1Mom/J, JAX stock #002216) mice were purchased from The Jackson Laboratory (Bar Harbor, ME, USA). Mice were bred and maintained at the Institute of Experimental

Medicine's conventional animal facility. All mice were 6-8 weeks old at the beginning of the experiments and both male and female mice were included. All protocols were approved by the Institute of Experimental Medicine animal ethics committee (approval #084/2020) and adhered to the Association for Research in Vision and Ophthalmology Statement for the Use of Animals in Ophthalmic and Vision Research. Since DED is more prevalent and more severe in women(45), and consistently, female mice develop worse DED than their male counterparts(46), we performed all experiments using equal numbers of female and male animals to consider this difference and we included sex as a variable in the analysis.

2.2 Reagents and antibodies

Unless otherwise specified, all chemical and biological reagents were from Sigma-Aldrich (Buenos Aires, Argentina). Table 1 lists all antibodies and the most significant reagents.

Table 1 – Reagents and antibodies

Reagent/Antibody	Product #	Concentration/dilution	Supplier
Dextran-fluorescein isothiocyanate	FD4-100MG	10 mg/ml in PBS	Sigma-Aldrich (Buenos Aires, Argentina)
Ketamine	Ketonal 50	100 mg/kg	Richmond Vet (Grand Bourg, Argentina)
Xylazine	Xilacina 20	10 mg/kg	Richmond Vet (Grand Bourg, Argentina)
Alexa Fluor® 488 anti-tubulin β3	801203	2.5-3.5 µg/ml	BioLegend (San Diego, CA, USA)
Alexa Fluor® 594 anti-mouse/human Ki-67	151213	0.5 µl/100 µl	BioLegend (San Diego, CA, USA)
Alexa Fluor® 647 anti-mouse/human CD324 (E-cadherin)	147308	2.5 µg/ml	BioLegend (San Diego, CA, USA)
Wheat Germ Agglutinin (WGA) Alexa Fluor® 647 Conjugate	W32466	10 µg/ml	ThermoFisher (Buenos Aires, Argentina)
Live/Dead Fixable Dead Cell Stain	L10119	1:500 in PBS	ThermoFisher (Buenos Aires, Argentina)
CD45 APC	103112	0.5 µl/100 µl	BioLegend (San Diego, CA, USA)
CD4 FITC	100406	0.5 µl/100 µl	BioLegend (San Diego, CA, USA)
CD8 Pacific Blue	100725	0.5 µl/100 µl	BioLegend (San Diego, CA, USA)
CD3 PE	100206	0.5 µl/100 µl	BioLegend (San Diego, CA,

			USA)
B220 PE-Cy7	103210	0.5 µl/100 µl	BioLegend (San Diego, CA, USA)

2.3 Lacrimal gland excision surgery

Mice were anesthetized by i.p. injection of ketamine (100 mg/kg) and xylazine (10 mg/kg) and placed on a heated pad. Excision surgery comprised four steps: 1) a 3-mm-long incision was made along the middle third of the line joining the lateral canthus of the ear and the pinna; 2) the superior pole of the extraorbital lacrimal gland was exposed by incising the ensheathing fibrous capsule; 3) the lacrimal gland was pulled out gently and excised taking special care not to damage the blood vessels next to its inferior pole; 4) the skin was closed using 6-0 nylon thread. The glands from both sides were excised sequentially. Sham surgery consisted only of steps 1 and 4. In all cases, a single dose of 10 mg/kg diclofenac sodium was injected s.c. in the scruff for postoperative analgesia, and ciprofloxacin ointment was applied over the wound once the surgery was completed. The eyes were protected from desiccation with sodium hyaluronate 0.4% (Dropstar LC, Laboratorio Poen, Argentina) until the mice recovered from anesthesia.

2.4 Tear production measurements

Tear production was measured by inserting a 1 mm-wide phenol-red impregnated filter paper strip in the inferior conjunctival fornix adjacent to the lateral canthus, where it was held in place for 60 seconds while restraining the mouse gently and allowing for normal blinking. The wetted length of the right eye of each mouse was measured (in mm) and used as one data point.

2.5 Assessment of corneal epithelial barrier function

Corneal fluorescein uptake was measured as previously described(43,47). In brief, 0.5 µl of dextran-fluorescein isothiocyanate (average molecular weight 3000–5000, 10 mg/ml in PBS) was applied to each eye and then the mouse was returned to its cage. After 3 min, a 10-second-long video of each eye under blue light was captured with the aid of a fluorescence-adapted dissection microscope (NightSea SFA-RB, Electron Microscopy Sciences, Hatfield, PA, USA). For analysis, a masked observer (AV) exported a representative video frame as an image and selected the exposed corneal area suitable for analysis as the region of interest by excluding reflections and other artifacts using ImageJ software (version 2.15.0, https://imagej.net/software/fiji/). Then, the green channel was extracted and the mean fluorescence intensity within the region of interest was calculated after background subtraction (50-pixel rolling ball radius), and the average of both eyes was used for analysis.

2.6 Assessment of corneal mechanical sensitivity

Mechanical thresholds were determined using a mouse-adapted version of Cochet-Bonnet esthesiometry(41,48). Nylon 6-0 monofilament was cut into segments of varying lengths (1.0 to 5.5 cm in 0.5 cm steps). With the mouse held firmly in one hand, the cornea was touched six times with each filament, starting with the longest segment. A positive response was defined as blinking and retracting the eye in reaction to at least three of the six tries. The longest segment yielding a positive response was used as the sensitivity threshold, and the average of both eyes was used for analysis. Corneal sensitivity was measured in the morning (8–11 AM) before any other experimental manipulation.

2.7 Spleen cell collection and $CD4^+$ T cell purification

Spleens were collected in 5 ml of serum-free RPMI 1640 medium and rendered into cell suspensions by gently pressing through nylon mesh using a syringe plunger; then, red blood cells were lysed with ammonium chloride–potassium buffer, and finally, $CD4^+$ T cells were isolated by negative selection with the aid of magnetic beads (MojoSort™ Mouse CD4+ T Cell Isolation Kit, BioLegend #480033) following the manufacturer's instructions. Cell purity was confirmed through flow cytometry $CD4^+$ immunostaining (>98% $CD4^+$ cells). Each *Rag1*KO mouse received $1x10^6$ cells in 0.5 ml PBS through intraperitoneal injection for adoptive transfer.

2.8 Lymph node cells and flow cytometry analysis

Cervical lymph nodes were harvested after euthanasia and rendered into a cell suspension by mechanical dissociation through nylon mesh. The cells were stained with a fixable viability dye (#L34975, Thermo Fisher Scientific, Buenos Aires, Argentina), washed, Fc-blocked (#158002, Biolegend), then stained for surface markers (B220 PE-Cy5 #103210, CD3 PE #100206, CD4 FITC #100406 and CD8 Pacific Blue #100725, Biolegend), and finally fixed with 1% formaldehyde in PBS. The entire cell suspension resulting from one mouse was stained and acquired as one independent sample on a Cyflow space cytometer (Partec, Germany) and analyzed using FlowJo software (FlowJo v10.3, Treestar, Ashland, OR, USA). First, singlets were gated based on forward scatter height versus area, then gated on side scatter height versus side scatter area, and finally gated on viability dye-excluding events (viable cells).

2.9 Preparation and flow cytometry analysis of conjunctival cell suspensions

Conjunctivas were collected in serum-free RPMI 1640 medium and minced with the aid of scissors and then incubated in collagenase 1 mg/ml in PBS at 37◦C with gentle shaking for 30 min, then DNAse 2 U/ml was added and the tissue samples were digested for an extra 15 min. EDTA (2 mM) and fetal calf serum (10%) were added to stop digestion, then the suspension was filtered and washed. Cells were stained with a fixable viability dye (#L34975, Thermo Fisher Scientific, Buenos Aires, Argentina), washed, Fc-blocked (#158002, Biolegend), then stained for surface markers

(CD45 APC #157606 and CD4 FITC #100406, Biolegend), and finally fixed with 1% formaldehyde in PBS. The entire cell suspension resulting from one mouse was stained and acquired as one independent sample. First, singlets were gated based on forward scatter height versus area, then gated on side scatter height versus side scatter area, then gated on viability dye-excluding events (viable cells), and finally on $CD45^+$ $CD4^+$ events.

2.10 Collection of eye tissue for imaging

After euthanasia, the conjunctival tissue of each eye was excised as two strips (superior and inferior) under a dissection microscope and collected in an ice-cold fixative solution. Immediately after, enucleation was performed by gently proptosing the eye globe and cutting the optic nerve with curved scissors. The two eyes of each mouse were collected in ice-cold fixative solution. Mice were euthanized one at a time so that all ocular tissue was collected within 5 min of the time of death to ensure adequate corneal nerve preservation(49).

2.11 Conjunctival sample staining, spinning disk scanning microscopy, and image analysis

Excised conjunctivas were fixed in pre-chilled 4% formaldehyde in PBS for 1 h, then washed 3 times with PBS, and stored at 4°C until processing. Conjunctiva samples were simultaneously blocked and permeabilized with a 1% BSA and 0.3% Triton X-100 solution overnight at 4°C, then washed, and stained overnight with wheat germ agglutinin Alexa Fluor® 647 Conjugate (#W32466, Thermo Scientific). The stained conjunctivas were washed three times in PBS for 20 min, mounted in Aqua-Poly/Mount (PolySciences), and stored at 4°C until imaged.

Image acquisition was performed with an Olympus IX83 inverted motorized microscope (Olympus, Tokyo, Japan) equipped with a UPlanSapo 10x/0.4 objective and a Disk Scanning Unit. Due to the irregularity in the distribution of conjunctival goblet cells within the conjunctival surface, composite images spanning the entire conjunctival strips were obtained using the multiple image alignment module of the cellSens Dimensions software (Olympus).

Images were acquired as Z-stacks with a 3-µm step size to ensure that all goblet cells within the conjunctival epithelium were included. To assess the area occupied by goblet cells, maximum intensity projections including all epithelial slices within the stacks were created using ImageJ. Then, the entire conjunctival surface was demarcated as the area of interest using the polygon selection tool, a background correction (20-pixel rolling ball radius) was applied, the image was thresholded, and finally, the percentage of the selected area occupied by the wheat germ agglutinin-derived signal was measured by the software.

2.12 Corneal immunostaining and confocal laser scanning microscopy acquisition

Eyes were processed as described by Yun et al(50). In brief, eyes were fixed in a pre-chilled formaldehyde-containing buffer for 75 min, washed, and stored in methanol at -20 °C until processed for staining. Then, the fixed corneas were cut from the back of the eye under a

dissection microscope, washed 3 times for 10 min and permeabilized with 1% Triton X-100 in PBS for 1 h, blocked overnight with 1% BSA, 0.3% Triton X-100 and Tween 0.01% in PBS, and stained overnight with Alexa 488-conjugated Alexa Fluor® 488 anti-tubulin β3, Alexa Fluor® 594 anti-mouse/human Ki-67 and Alexa Fluor® 647 anti-mouse/human CD324 (E-cadherin) antibodies (#801203, # 151213 and #147308, BioLegend). Each batch of anti-tubulin β3 antibody was titrated before use to minimize background staining, usually resulting in 0.5 µl antibody/100 µl buffer/cornea (2.5 µg/ml) as optimal. The stained corneas were washed three times for 60 min in PBS–Tween 0.1%, counterstained with 1 µg/ml DAPI, mounted flat with the aid of relaxing cuts in Aqua-Poly/Mount (PolySciences), and stored at 4 °C until imaged.

Image acquisition was performed with a FluoView FV1000 confocal microscope (Olympus, Tokyo, Japan) equipped with Plapon 60X/1.42 and UPlanSapo 20X/0.75 objectives. Z stacks (0.5-µm step size) spanning the entire corneal epithelium (approximately 30 µm) were obtained at two opposite located at 600 µm from the center (defined as the center of the nerve whorl or as the center of the disorganized area in those samples with highly disrupted nerve whorls). Corneal nerve analysis was performed at three different levels within the corneal epithelium. For subapical nerve terminals, the first section located entirely beneath the apical epithelial squamous cells (1–1.5 µm deep, usually the third or fourth slice in the stack) was selected. Then, the image was thresholded after background subtraction (10-pixel rolling ball radius), and the percentage area occupied by nerve endings was determined by the corresponding ImageJ function. For mid-epithelial nerve terminals, the middle section between the apical- and basal-most epithelial sections from each stack was chosen. Then, the number of nerve endings was assessed after background subtraction (10-pixel rolling ball radius) by a masked observer (AV) using the Cell Counter ImageJ function. Data are shown as the number of terminals / 60X field (423.94 µm2 area). To analyze the complexity of the subbasal epithelial nerves, the Sholl plugin in ImageJ software was used. In brief, a maximum intensity projection of the 10 sections encompassing the corneal subbasal nerve mat was created, then the background was subtracted (50-pixel rolling ball radius), and the image was thresholded. Finally, 10 concentric circles with a 10-µm radius step size were traced at the center of the final image, and the resulting sum of intersections of tubulin β3 nerves for each concentric circle was calculated using the software and used for analysis(51).

For epithelial cell turnover analysis, a blind observer (AV) selected a single section from the Z-stack encompassing the basal epithelial cells and manually counted the number of Ki-67^{+} cells. Side views where obtained using the Orthogonal Views function of ImageJ.

2.13 RNA isolation from trigeminal ganglia and RNA-Seq analysis

The trigeminal ganglia were dissected after euthanasia and cardiac perfusion with PBS to remove contaminating blood cells(52), collected in ice-cold TRI Reagent, and stored at -80°C until processing. For RNA isolation, both trigeminal ganglia from one mouse were homogenized in 1 ml of TRI Reagent, and then 0.2 ml of isopropanol was added. After centrifugation, RNA was purified

from the aqueous phase using the Direct-zol RNA MiniPrep kit (Cat #R2052, Zymo Research, Irvine, CA, USA) following the manufacturer's instructions. The concentration and purity of RNA were assessed with a NanoDrop 1000 spectrophotometer (ThermoFisher Scientific, Waltham, MA, USA). RNA-Seq was performed by NovoGene (Sacramento, CA, USA) using the Illumina NovaSeq platform to generate 150 bp paired-end reads. The sequenced reads were mapped to the mouse reference genome (assembly GRCm38/mm10) using STAR v2.7.11a, and the quantification of reads per gene was estimated by RSEM v1.3.1. Subsequent analyses were performed in R (v4.3.1). Gene filtering was performed by selecting features with >=10 reads in at least 3 samples. For quality controls, the filtered data were subjected to a principal component analysis and hierarchical clustering (Ward.D2 method, Euclidean distance) after trimmed mean of M-values normalization (edgeR v4.0.16). Gene information (ENSEMBL ID, external gene name and gene biotype) was extracted using biomaRt (v2.58.2). Differential gene expression analyses were performed by the DESeq2 methodology (v1.42.1). Genes with log2 fold change > 0.378 and adjusted p-value < 0.1 were considered as upregulated, and genes with log2 fold change < -0.378 and adjusted p-value < 0.1 were categorized as downregulated. The list of genes was ranked by log10 adjusted p-value * sign(log2 fold change) and subjected to a Gene Set Enrichment Analysis with the Gene Ontology database, using enrichGO and simplify (clusterProfiler v4.10.1). Enriched Gene Ontology terms with adjusted p-value of 0.05 were considered significant. All raw data files are available at ArrayExpress (https://www.ebi.ac.uk/biostudies/arrayexpress), accession E-MTAB-13945

2.14 Tear cytokine levels

To collect a tear washing sample, each mouse was manually restrained, then 5 µl of PBS+BSA 0.1% was applied on one eye using a 10-µl pipette tip, and finally the same volume was gently collected 20 seconds later from the ocular surface. The right and left eye washings from one mouse were pooled as one sample and stored at -80°C until processing. Cytokine levels were determined using a bead-based multiplex assay (LEGENDplex, #741048, BioLegend) following the manufacturer's instructions and are expressed as mean±SEM (pg/ml).

2.15 Statistical analysis

Student's t-test and one- or two-way analysis of variance (ANOVA) with Sidak's post hoc tests were used to compare the means of two or more samples, respectively. Significance was set at $p<0.05$ and two-tailed tests were used in all experiments. All data are shown as mean±SEM. Calculations were performed using GraphPad Prism version 9 software (GraphPad Software, La Jolla, Ca, USA).

3. Results

3.1 Impact of adaptive immunity deficiency on DED phenotype development

$CD4^+$ T cells are pathogenic in DED because they enhance desiccation-induced ocular surface inflammation by coordinating the local adaptive immune response(7,9–12,14,15). However, whether a $CD4^+$ T cell-coordinated adaptive immune response is required for either corneal epitheliopathy or neuropathy to develop in this disorder remains undetermined. To address this question, we compared the progression of the disease phenotype in immunocompetent wild-type (WT) and adaptive immunity-deficient *Rag1*KO (lacking $CD4^+$ and $CD8^+$ T, NKT, and B cells) mice using a surgical DED model (Figure 1A). This model involves the bilateral excision of the extraorbital lacrimal gland, the largest of the three glands that contribute to tear secretion in rodents. The resulting desiccation of the ocular surface then activates a pathogenic immune response, thus mimicking aqueous-deficient DED(53,54). All in vivo measurements were performed at baseline and on days 5 and 10 to assess progression, after which mice were euthanized because ocular signs of DED and the accompanying $CD4^+$ T cell response are fully developed at this time point(55,56).

First, we verified that the tear deficiency 5 days after surgery was comparable in both strains (Figure 1B) to ensure the validity of the *Rag1*KO DED model. Baseline tear production did not differ between strains nor between female and male mice that underwent either sham- or DED-inducing surgery (sex factor, <2% total variation, p=0.50). Also, the external eye phenotype in WT and Rag1KO did not appreciably change after 10 days of DED induction (Figure 1C). Next, we quantified conjunctival goblet cells because their loss is a clinically validated finding in DED that correlates with disease severity(57,58). Since the distribution of these cells within the conjunctiva is not uniform(59), we measured the total area occupied by goblet cells in low-magnification images obtained from conjunctival whole mounts (Figure 1D and top panels of E). As shown in Figure 1D, the total conjunctival goblet cell area did not differ between control mice (while DED induction led to a comparable loss of goblet cells in both strains. The DED-induced loss was more readily evident but comparable in magnitude when restricting the analysis to the goblet cell-rich area of the conjunctiva from both strains (Figure 1E, bottom panels). Altogether this data shows that both mouse strains develop comparable DED in terms of tear production and conjunctival goblet cell loss, and therefore, that the *Rag1*KO mouse is a valid model for assessing how the lack of adaptive immunity impacts the corneal aspects of the disease.

3.2 Adaptive immune deficiency does not impede DED-associated corneal epitheliopathy development

Corneal epitheliopathy is a hallmark clinical finding in DED, characterized by epithelial barrier dysfunction and accelerated cell turnover(4). Although it is accepted that type 1 and type 3 immunity contribute to corneal epithelial damage(12,19,25,28,30), whether the adaptive (T and B-cell dependent) component of the immune response is required for corneal epitheliopathy to

develop in DED is unclear. To answer this question, we first measured corneal dye uptake as a means to probe corneal barrier function(4,60). In DED, increased epithelial cell shedding and matrix metalloproteinase activity disrupt tight junctions, thus allowing the intercellular diffusion of fluorescein-tagged dextran(60). As shown in Figures 2A and 2B, DED WT mice developed a time-dependent increase in corneal dye uptake with the typical punctate staining pattern observed in patients(4,60). Remarkably, DED *Rag1*KO mice showed corneal dye uptake that was comparable to that of DED WT mice on days 5 and 10 of disease induction (Figure 2A) and with no appreciable differences in the staining pattern (Figure 2B). Sub-analysis by sex of the DED groups (Supplementary Figure 1A, 3-way ANOVA with factors strain, sex, and time) revealed that while time had the largest effect on corneal epitheliopathy development (60.7% of total variation, $p<0.0001$), female mice had worse epithelial disease than male mice of the same strain (sex factor accounted for 9.1% of total variation, $p<0.0001$) and strain had no significant overall effect (1.4% of total variation, $p=0.08$). Female WT mice with DED had more corneal dye uptake on day 5 ($p=0.01$) than female *Rag1*KO mice with DED but this difference disappeared by day 10 ($p=0.59$), suggesting a faster tempo (Supplementary Figure 1A).

Next, we quantified the number of proliferating corneal epithelial cells as an indicator of cell turnover rate, which increases in DED(61). As shown in Figures 2C and Supplementary Figure 1B, both WT and *Rag1*KO mice with DED had more proliferating ($Ki67^+$) corneal epithelial cells with no statistically significant difference between strains. Of note, proliferating cells were restricted to the basal epithelial layer in control mice while they also extended to the suprabasal layer in DED mice of both strains (Supplementary Figure 1C), a pattern consistent with DED-induced corneal epitheliopathy(61). These results suggest that the absence of an adaptive immune response does not condition the development of corneal epitheliopathy in this DED model.

3.3 Adaptive immune deficiency prevents DED-associated corneal neuropathy development

We have previously shown that antigen-driven $CD4^+$ T cell activation in an ocular surface that is not exposed to desiccation is sufficient to cause corneal nerve damage(43). However, other factors may also determine whether corneal nerve damage occurs in the context of an ocular surface immune response since $CD4^+$ T cell activation drives corneal nerve damage in herpetic keratitis and ocular graft-versus-host disease but not in allergic conjunctivitis mouse models(44). DED involves ocular desiccation and innate immune activation followed by an adaptive immune response. Thus, if local adaptive immunity is required for corneal nerve dysfunction to develop in DED is unknown. To address this question, we first measured corneal sensitivity to mechanical and capsaicin stimulation to probe two different types of nerve fibers in WT and *Rag1*KO with DED.

At baseline, *Rag1*KO mice showed slightly reduced corneal mechanosensitivity (-4.4±0.9%, Supplementary Figure 2A) and increased sensitivity to capsaicin (Supplementary Figure 2B) compared to WT mice. Sex had no significant effect ($p=0.58$, Supplementary Figure 2C) on baseline mechanosensitivity thresholds in both strains. Therefore, when evaluating the effects of

DED in each strain, the results were normalized to each strain-specific baseline (Figures 2D and 2E). DED WT mice developed a progressive reduction in corneal sensitivity and increased capsaicin sensitivity, as previously described(41,47), but this was not observed in DED *Rag1*KO mice. In contrast to corneal epitheliopathy where female sex was the strongest determinant of differences, sub-analysis by sex of the DED groups (Supplementary Figure 2D, 3-way ANOVA with factors strain, sex, and time) revealed that strain had the largest effect (22.3% of total variation, $p<0.0001$) on mechanosensitivity followed by time (14.3% of total variation, $p<0.0001$) while sex had a small significant effect (2.9% of total variation, $p=0.03$). Although the drop in corneal mechanosensitivity was greater in the females, WT mice of both sexes displayed reduced sensitivity on days 5 and 10 of DED induction (Supplementary Figure 2D).

Since corneal mechanosensitivity reduction in mouse DED models correlates with structural changes(38,39), we evaluated corneal nerve morphology on day 10 (Figures 2F-I and Supplementary Figure 2E) at three different levels within the intraepithelial innervation(43,47). DED WT mice had reduced corneal nerve density at the subapical, mid-epithelial, and subbasal levels. By contrast, nerve density in *Rag1*KO mice with DED did not significantly change at any of the three corresponding levels of intraepithelial corneal innervation (Figure 2F). The magnitude of corneal nerve changes in DED WT mice decreased from the superficial subapical level to the deeper subbasal level, and DED *Rag1*KO mice showed a similar but not significant trend (Supplementary Figure 2F). Altogether, the data indicates that corneal nerve damage requires an adaptive immune response to develop in the context of DED.

3.4 DED induces a trigeminal transcriptomic signature related to corneal nerve damage only in adaptive immune-sufficient mice

Corneal nerve fibers are the terminal projections of the somatosensory neuronal bodies located in the trigeminal ganglion, and many studies have shown that injury to the peripheral nerve endings of extraocular tissue-innervating trigeminal neurons leads to reactive gene expression changes(62–64). To further study the impact of adaptive immune deficiency on corneal neuropathy development, we analyzed the transcriptional profiles of the trigeminal ganglia of the same mouse groups by bulk RNA-sequencing. We determined the effect of DED on trigeminal gene expression separately in the two strains using the same-strain sham-treated group as a reference, and then we compared samples from WT DED and *Rag1*KO DED mice. A complete list of differentially expressed genes can be found in Supplementary File 1.

After 10 days of DED induction, there were 172 differentially expressed genes (DEGs) in WT mice, of which 77 were up-regulated and 95 were down-regulated, whereas there were only 7 DEGs (5 up- and 2 down-regulated) in *Rag1*KO mice (Figures 3A and 3B). Up-regulated genes in WT DED mice included: *Atf3*, *Sprr1a*, and *Fos*, three canonical regeneration-associated genes induced by axonal injury in peripheral nervous system neurons(65); *Mbp*, which encodes myelin basic protein and is induced during the Schwann cell response to nerve injury(66); and *Sparc*, a matricellular protein secreted by glial cells that modulates axonal regeneration(67).

Down-regulated genes in WT DED mice included: *Trpm8*, *Trpa1*, and *Piezo2*, three cation channels involved in corneal thermo- and polymodal nociception and mechanosensation(38); *Asic1* and *Asic3*, acid-sensing cation channels expressed in trigeminal neurons that participate in nociception(68); *Pirt*, a positive regulator of transient receptor potential vanilloid-1 channel activity in nociceptive neurons(69); *Kcnk18*, *Scn10a*, *Scn4b*, and several other voltage-gated potassium and sodium channels that determine sensory neuron excitability and are involved pain syndromes(70); and *L1cam* and *Sema4f*, which guide axonal growth(41). *Cd74* was the only DEG that was up-regulated in both WT and *Rag1*KO samples: it encodes the macrophage-inhibitory-factor receptor and its expression in the trigeminal ganglion has been mapped to macrophages and neutrophils(71). The remaining 4 up-regulated DEGs in *Rag1*KO mice were: *Smoc2* (a matricellular protein related to *Sparc*) and *S100a4* (a cytoskeleton-interacting protein), both of which are induced by nerve injury, and *Pmp2*, which encodes peripheral myelin protein 2 and its regulation is linked to *S100a4*(72).

Analysis of DEGs between trigeminal ganglia from WT and *Rag1*KO mice with DED revealed 34 up-regulated and 39 down-regulated genes in WT mice (Supplementary Figure 3). Several up-regulated DEGs in WT mice corresponded to the absent adaptive immune response in the *Rag1*KO strain and were mostly B-cell related: *Igkc* (Ig kappa constant domain), *Fcer2a* (low affinity IgE Fc receptor), *Iglc2* (Ig lambda constant 2), *Cd19*, *Ly6d* (T and B cell marker), Il7r (IL-7 receptor), Spib (lymphoid transcription factor), *Fcmr* (IgM Fc receptor), *Cd79a*, *Cd79b*, *Ighm* (IgM heavy constant), and *Sell* (CD62L). The 3 DEGs that were up-regulated in WT DED mice relative to both sham WT and DED *Rag1*KO mice were *Npy* (neuropeptide Y), *Dbp*, and *mt-Atp6*, all of which are associated with trigeminal neuropathic pain(63,73). Down-regulated genes in WT DED mice included *Asic3* (acid-sensing cation channel 3), voltage-gated sodium channels *Slc7a7* and *Scn10a*, and neuronal excitability regulators *Tmem63c*, *Tmem25*, and *Tmem132e*, all of which were also down-regulated relative to sham WT mice, and the axon-guiding semaphorin *Sema3f*.

Gene set enrichment analysis found that DED affected 189 pathways in WT mice and 24 pathways in *Rag1*KO mice (Supplementary Figure 4). In WT mice, the 10 most significantly activated pathways pertained to pre- and postsynaptic translation, the humoral immune response, and antigen processing and presentation while the 10 most significantly suppressed pathways related to microtubule-based transport, exocytosis, detection of abiotic stimuli, and those involved in sensory perception of pain. In *Rag1*KO mice, the 10 most significantly pathways activated by DED related to presynaptic translation and regulation of antigen processing and presentation whereas the 10 most suppressed ones were dendrite development, regulation of transporter activity, synapse assembly, and potassium ion transport, albeit the statistical significance was 10-fold lower than in WT mice. Altogether, these findings indicate that DED induces trigeminal gene expression changes that are more profound and more related to corneal nerve damage in WT than in *Rag1*KO mice, which is consistent with the lack of corneal neuropathy development in the latter group.

3.5 DED leads to sustained proinflammatory cytokine levels in tears only in adaptive immune-sufficient mice

The adaptive immune response, and specifically its $CD4^+$ T cells, sustain ocular surface inflammation in DED by releasing Th1 and Th17-associated pathogenic cytokines(13,15,19,31,56,74–76). Having observed that the corneal nerves were spared by DED in adaptive immune-deficient mice, we hypothesized that the specific lack of $CD4^+$ T cells and their associated cytokines coordinating the local immune response in this strain could explain the absence of DED-associated corneal neuropathy. Therefore, we analyzed cytokine levels in tear washings from WT and *Rag1*KO mice on day 10 of DED induction, a time at which the $CD4^+$ T cell response has fully ensued(11,56)(Figure 4). In WT mice, DED increased the levels of 6 of the 7 tested cytokines (IFN-γ, TNF, IL-6, IL-10, IL-17A, and IL-22). By contrast, *Rag1*KO mice with DED did not have increased tear levels of any of the 7 cytokines on day 10 when compared to control mice of the same strain. Subanalysis by sex of the WT strain data revealed that female DED mice had higher tear levels of IL-17A ($p=0.03$) and a similar trend for IFN-γ ($p=0.07$) while the other tested cytokines did not differ between sexes. Our data highlights the pivotal role that the adaptive immune response plays in amplifying and sustaining ocular surface inflammation in DED through cytokine production.

3.6 Adoptive transfer of $CD4^+$ T cells from DED mice recapitulates ocular phenotype and corneal nerve damage but not epitheliopathy in the recipients

Our results so far supported our hypothesis that the adaptive immune response drives corneal nerve damage in DED. Based on our previous observation that isolated ocular $CD4^+$ T cell activation is capable of inducing corneal neuropathy(43), we hypothesized that the lack of $CD4^+$ T cells in *Rag1*KO mice was responsible for their resistance to develop corneal nerve damage in the context of DED. To test this, we isolated splenic $CD4^+$ T cells from control or DED WT mice 10 days after surgery and transferred them into sex-matched naïve *Rag1*KO mice, which were then assessed weekly for DED pathology (Figure 5A). First, we validated the model: $CD4^+$ T cells from control or DED WT did not significantly differ in the proportion of Th1 or Th17 cells, although there was a trend towards more IFN and IL-17A production in the latter group (Supplementary Figure 5A). Also, to rule out a potentially confounding effect of contaminating $CD8^+$ T or B cells that may proliferate rapidly in the lymphopenic host, we used flow cytometry in lymph nodes of the recipient mice 4 weeks after transfer to quantify these cells. We confirmed that the recipient *Rag1*KO mice were effectively reconstituted only with $CD4^+$ T cells (Figure 5B). Then, we verified the functionality of the transferred $CD4^+$ T cells by assessing their migration to the ocular surface. As previously reported(11), DED-induced $CD4^+$ T cells were more efficient than control $CD4^+$ T cells at homing to the conjunctiva in the recipient mice (Figure 5C and Supplementary Figure 5B). Despite the conjunctival infiltration, no appreciable changes in external eye phenotype (Figure 5D) were observed, as is the case for the surgically induced DED model (Figure 1B). As a final validation step, we evaluated the pathogenicity of transferred $CD4^+$ T cells by assessing their effect on tear

production and conjunctival goblet cells. *Rag1*KO mice that received $CD4^+$ T cells from DED WT donors had decreased tear production compared to *Rag1*KO mice that received control $CD4^+$ T cells (Figure 5E), in line with the increased lacrimal gland infiltration described in a similar model(11). In addition, DED $CD4^+$ T cell-recipient mice exhibit decreased conjunctival goblet cell density compared to control recipient mice (Figures 5F and 5G), thus reproducing all the non-corneal findings observed in WT and *Rag1*KO with surgically-induced DED (Figure 1).

Once we established the validity of this adoptive transfer model, we assessed the capacity of the pathogenic $CD4^+$ T cells to cause corneal epithelial damage in the recipient mice in the absence of desiccating stress. As shown in Figures 6A-B, neither group of recipient mice (control and DED-induced $CD4^+$ T cells) showed a change from baseline levels of corneal dextran-FITC uptake. Sub-analysis by sex (Supplementary Figure 6A, 3-way ANOVA with factors transferred cells, sex, and time) confirmed that no factor had a significant effect on corneal epitheliopathy development (<5% of total variation, $p>0.05$). Moreover, both groups of recipient mice had comparable numbers of proliferating corneal epithelial cells (Figures 6C and Supplementary Figure 6B) that were restricted to the basal layer (Supplementary Figure 6C), as observed in homeostatic conditions. Thus, these findings indicate that in the absence of desiccating stress, $CD4^+$ T cells from DED mice are not sufficient to induce corneal epitheliopathy in *Rag1*KO recipient mice.

In parallel to corneal epitheliopathy assessments, we evaluated corneal sensitivity as an indicator of corneal nerve function. Contrasting with corneal epithelial barrier function results, corneal mechanosensitivity significantly decreased in the DED-induced $CD4^+$ T cell-recipient mice as early as 7 days after transfer (Figure 6D). Of note, in this group the sensitivity thresholds did not worsen significantly from day 7 until the end of the experiment (day 28). Moreover, sub-analysis by sex (Supplementary Figure 6D, 3-way ANOVA with factors group, sex, and time) revealed that sex had no effect ($p=0.88$) on mechanosensitivity, in contrast with the findings from the surgical DED model (Supplementary Figure 2A). Finally, we analyzed corneal nerve morphology on day 28 post transfer and found reduced intraepithelial nerve density in the DED-induced $CD4^+$ T cell-recipient mice at the three levels analyzed: subapical nerve endings, mid-epithelial vertical fibers, and subbasal nerves (Figures 6E-H). The pattern of change in DED-induced $CD4^+$ T cell-recipient mice was similar to that observed in WT mice with DED: a larger relative reduction in the subapical nerve endings than in the subbasal corneal nerves (Supplementary Figure 6E). Altogether these results show that adoptive transfer of pathogenic DED-induced $CD4^+$ T cells reproduces corneal neuropathy but not epitheliopathy in recipient mice.

3.7 Adaptive immune-deficient mice reconstituted with naive $CD4^+$ T cells gain the ability to develop corneal nerve damage upon DED induction

To confirm that $CD4^+$ T cells drive corneal nerve damage in DED, we tested if reconstitution of *Rag1*KO mice with naive $CD4^+$ T cells was sufficient to enable corneal neuropathy development upon surgical DED induction. To this aim, we isolated $CD4^+$ T cells from naive WT mice and transferred them by i.p. injection into *Rag1*KO mice that, one week later, underwent either bilateral

extraorbital lacrimal gland excision or sham surgery as control (Figure 7A). First, we confirmed that T cell reconstitution in the cervical lymph nodes was effective and limited to $CD4^+$ T cells (Figure 7B), and then, we tested for the development of corneal epitheliopathy and neuropathy after surgical DED induction. We found that corneal barrier disruption progressively increased on days 5 and 10 of DED induction (Figure 7C and 7D) and to an extent comparable to WT and *Rag1*KO mice with DED (Figure 2A). However, and contrasting with *Rag1*KO mice lacking T and B cells, $CD4^+$-reconstituted DED *Rag1*KO mice developed progressive loss of corneal mechanical sensitivity (Figure 7E). Concordantly, we found reduced corneal nerve density at the subapical, mid-epithelial, and subbasal levels in $CD4^+$-reconstituted mice with DED compared to $CD4^+$-reconstituted mice that underwent sham surgery (Figures 7F-I). The pattern of change in $CD4^+$-reconstituted mice with DED showed a larger relative reduction in the subapical nerve endings than in the subbasal corneal nerves (Figure 7J). These results altogether show that reconstitution of *Rag1*KO mice with naïve $CD4^+$ T cells from WT mice followed by surgical DED induction enables corneal neuropathy onset and progression, thus confirming that $CD4^+$ T cells are required for corneal nerve damage to develop in the setting of DED disease.

4. Discussion

Our current understanding of DED involves dysfunctional tear film-instigated corneal epitheliopathy and neurosensory abnormalities as defining clinical features and ocular surface inflammation as a key driver of the disease process(3,4,6). Contrasting with the numerous studies into the pathogenesis of corneal epitheliopathy in DED, the mechanisms underlying corneal nerve damage are poorly understood(38). A $CD4^+$ T cell-driven adaptive immune response perpetuates ocular surface inflammation(8) and thus interfering with $CD4^+$ T activation is the target of several approved therapies for DED in patients. However, whether $CD4^+$ T cells are required for either DED-associated corneal epitheliopathy or neuropathy to occur is undetermined. Herein we show that while DED-associated corneal epitheliopathy develops unimpeded in the absence of $CD4^+$ T cells, corneal nerve damage does not. Thus, our findings indicate that the mechanisms behind these two defining aspects of the disease are different and that therapies that target one may not necessarily tackle the other in the multifactorial pathogenesis of the DED.

Our finding of corneal epitheliopathy developing independently of $CD4^+$ T cell activation might seem to contradict the literature on DED pathogenesis(7,8), but a meticulous analysis of the published reports reveals otherwise. The contribution of a $CD4^+$ T cell-driven adaptive immune response to DED progression was established almost two decades ago by showing that the adoptive transfer of $CD4^+$ T cells from DED mice reproduces lacrimal gland- and conjunctival infiltration in T cell-deficient recipients(11). This study, however, did not report corneal barrier disruption in the recipient mice, a hallmark of corneal epitheliopathy. Subsequent investigations demonstrated the pathogenic relevance of type 1 (Th1) and type 3 (Th17) immunity in many aspects of DED including corneal epitheliopathy(13,15,19,30,31,34,56,74–77), but none has

indicated that corneal epitheliopathy does not occur in the absence of $CD4^+$ T cell activation. One study indicated that local depletion of dendritic cells and macrophages prevents conjunctival $CD4^+$ T cell infiltration and goblet cell loss but did not describe any effect on corneal epitheliopathy-related signs(13). Our findings are in complete agreement with these reports: adoptive transfer of $CD4^+$ T cells from WT mice with DED reproduces lacrimal gland dysfunction, conjunctival infiltration and conjunctival goblet cell loss in T cell-deficient recipient mice (Figures 5 and 6). Another landmark study showed that the adoptive transfer of effector memory $CD4^+$ T cells from female mice with DED into naïve recipients leads to more severe corneal epitheliopathy than when naïve or effector $CD4^+$ T cells from the same donor mice are transferred, but in all cases corneal epithelial changes developed only after desiccating stress exposure(56). Our findings are also in line with this report, as female WT mice (with $CD4^+$ T cells) in our study developed more severe corneal epitheliopathy than female *Rag1*KO mice (without $CD4^+$ T cells) on day 5 of DED induction, but the differences disappeared by day 10 among strains and sexes (Supplementary Figure 1). Another report observed no corneal barrier disruption in *Rag1*KO mice subjected to desiccating stress for 5 days, and this resistance to corneal epitheliopathy development was overcome by prior adoptive transfer of Th17 but not Th1 $CD4^+$ T cells from WT mice with DED(78). However, this study employed milder and shorter ocular desiccation treatment (5 days), potentially selecting for the least pathogenic conditions. At any rate, none of the studies outlined above reported that the adoptive transfer of $CD4^+$ T cells without additional ocular desiccation leads to corneal epitheliopathy development in the recipient mice. Consistently, the present study indicates that $CD4^+$ T cells are dispensable for DED-associated corneal epitheliopathy onset, but these cells may accelerate or worsen this aspect of the disease in females.

Our data showing that $CD4^+$ T cells are not required for corneal epithelial damage to occur in DED does not imply that type 1 and 3 immunity are not involved in this aspect of the disease. IFN-γ and IL-17 are pathogenic to the corneal epithelium(19,27,29), and conjunctival NK cells and other innate immune cells represent a significant source of these cytokines in the ocular surface(30,34–37). Using a non-surgical DED model, Coursey et al.(35) showed that conjunctival IFN-γ and Th1-associated chemokines in *Rag1*KO mice increase after 5 days of desiccating stress but return to baseline levels by day 10. These authors also observed conjunctival goblet cell loss in *Rag1*KO mice after 5 days of DED induction, indicating that early IFN-γ production by innate immune cells in the ocular surface is sufficient to cause this typical DED finding(26,35). The present study complements these prior reports by showing that DED-induced conjunctival goblet cell apoptosis, which is induced mainly by IFN-γ(12,26), occurs unimpeded in the absence of $CD4^+$ T cells (Figures 1D and 1E). Of note, we did not detect increased tear levels of IFN-γ and IL-17 in T cell-deficient mice after 10 days of DED induction (as opposed to WT mice, Figure 5), indicating that $CD4^+$ T cells are required for sustained production of these pathogenic cytokines in the DED-affected ocular surface, as previously shown by others(56). Thus, our findings also suggest that the early innate components of type 1 and type 3 responses are competent to prime the

proinflammatory ocular surface state and conjunctival goblet cell dysfunction that contribute to corneal epithelial damage.

In contrast to corneal epitheliopathy, we observed that the onset of corneal nerve damage in the setting of DED is entirely dependent on the presence of $CD4^+$ T cells. Basal corneal epithelial cells ensheath the subbasal nerves within infoldings of their cell membrane, thus serving as surrogate Schwann cells to the intraepithelial corneal fibers by providing physical and metabolic support(40). Considering the intimate relationship between corneal epithelial cells and nerve fibers, it is striking that desiccation-induced pathologic changes in the former may occur while the latter remain unaffected in the absence of $CD4^+$ T cells. However, we have found that the converse is also true: corneal nerves may be damaged by $CD4^+$ T cell activation in the ocular surface while the corneal epithelium remains unaffected in the absence of desiccating stress(43). Thus, the present findings extend the notion of an epithelial-neural divide in corneal pathology to DED disease. Since the pathogenic mechanisms that drive the corneal epithelial aspect of the disorder are clearly different from the ones that cause its neural manifestations, this might translate to variations in the immune and non-immune components of DED contributing to the diverse presentations of the disease. In line with this, one study found little to no difference in the extent of corneal epithelial changes (as assessed by in vivo confocal microscopy) between Sjögren's and non-Sjögren's syndrome DED patients(79). By contrast, two studies reported worse changes in corneal nerve morphology (also by in vivo confocal microscopy) in Sjögren's than in non-Sjögren's syndrome DED patients(79,80). The sensitivity of corneal nerves to $CD4^+$ T cell activation could also explain the corneal neuropathy findings that correlate with the severity of the systemic autoimmune disease in rheumatoid arthritis patients(81) or that are observed after recovery in COVID-19 patients(82).

The trigeminal transcriptomic signatures observed after 10 days of DED induction are consistent with the extent of corneal nerve damage in wild-type and *Rag1*KO mice (Figure 3 and Supplementary Figures 3 and 4). Gene expression changes in DED WT mice but not in *Rag1*KO mice correspond to the common transcriptomic signatures of nerve injury and regeneration and neuropathic pain: up-regulation of transcription factors *Atf3* and *Fos* and neuropeptide Y, and altered ion channel expression(65,83). Based on the number of DEGs and the fold-change in expression, the magnitude of the DED-induced transcriptomic signature in the trigeminal ganglion is smaller than those reported for other models of trigeminal nerve injury(62–64,84). However, most models involve whole nerve ligation or injection of inflammatory agents whereas DED targets the peripheral nerve endings of only 2% of trigeminal neurons(38). A combined analysis of bulk- and single-cell RNA-seq studies of dorsal root ganglia in neuropathic pain or nerve injury models showed that most gene expression changes take place in nociceptor neurons, and that the reduced magnitude of expression changes in whole ganglion studies probably relates to the diluting effect of other cell types(83). In light of this, the qualitatively comparable trigeminal transcriptomic signature observed after 10 days of DED in WT mice in our study probably indicates

a pain maintenance period as that reported after 10 days of partial infraorbital nerve transection(84). Functional impairment of mechanical sensitivity, capsaicin hypersensitivity, spontaneous ocular pain, and morphological alterationsin corneal nerve fibers are well established at this time point in our model(47). These findings are consistent with the gene expression changes involving detection of noxious stimuli, neuronal excitability and signal transduction, nerve repair, and the immune response found in the trigeminal ganglion of DED WT mice, which are associated with a neuropathic pain state in other models(83,84). Supporting this hypothesis, the up-regulation of the macrophage-specific marker *Cd74* in both DED WT and *Rag1*KO mice probably reflects the increase in neuron-associated macrophages in the trigeminal ganglion upon axonal injury that relates to neuropathic pain(71,85). Thus, our data support the notion that adaptive immune response contributes to the development of neuropathic pain in the setting of DED.

Although our study does not delve into the exact process by which $CD4^+$ T cells promote corneal neuropathy, it is tempting to speculate that the elevated tear cytokine levels in WT but not in *Rag1*KO mice after 10 days of desiccating stress play a role (Figure 5). $CD4^+$ T cells coordinate immune responses in tissues mostly by secreting cytokines that have diverse effects on innate immune cells and non-immune cells(23,24). In DED, conjunctival $CD4^+$ T cells increase in number and constitute a likely source of the Th1 and Th17 cytokines that reach the cornea through the tear film. We observed more severe disruption of the superficial subapical nerve endings than of subbasal nerve fibers in the three models tested, one of which lacked ocular desiccation and relied entirely on $CD4^+$ T cell activation for ocular pathogenicity. This pattern of nerve fiber impairment is compatible with a soluble factor diffusing from the tear film into the corneal epithelium, which could be an action-at-distance effect of conjunctival $CD4^+$ T cells. In line with this hypothesis, we observed increased conjunctival infiltration after transferring DED-induced $CD4^+$ T cells into *Rag1*KO mice (Figure 6C). Nonetheless, a smaller number of T cells patrol the corneal epithelium under homeostatic conditions in humans and mice(86) and may even establish corneal tissue residency in pathologic settings(87). Therefore, it remains to be established whether $CD4^+$ T cells must enter the cornea to exert their pathogenic action on corneal nerves or if they do so at a distance from the surrounding conjunctiva in DED disease, and the exact role of inflammatory tears in this process.

Finally, female sex is the most influential risk factor for DED in patients(88,89), and our findings also shed light on this association: female mice develop worse DED in terms of corneal epithelial and neural impairment in part due to greater pathogenic activity of $CD4^+$ T cells in this sex (Supplementary Figures 1 and 2). However, the difference in disease severity between sexes cannot be solely attributed to these cells because female mice adoptively transferred with $CD4^+$ T cells from female DED mice do not develop worse corneal neuropathy than their male counterparts (Supplementary Figure 6A), indicating that sex influences other pathogenic factors that are triggered by desiccation in the ocular surface. In line with this, a reduced regulatory role of ocular surface neutrophils in female mice has been linked to an amplified effector $CD4^+$ T cell response in

the ocular surface and worse DED phenotype(90). Alternatively, the more severe corneal mechanosensitivity impairment in female mice with DED (Supplementary Figure 2A) may involve greater susceptibility of corneal nerves to immune-mediated damage than in males. Supporting this idea, corneal neural repair mechanisms are conditioned by sex as female mice exhibit faster corneal neuroregeneration than their male counterparts(91).

In summary, the present study contributes to our understanding of the pathophysiology of DED-associated corneal epithelial and nerve damage by showing that desiccation-induced changes in the distal subapical endings of corneal nerves require the activation of $CD4^+$ T cells while those in corneal epithelial cells occur independently of the adaptive immune response. One limitation of our study (and of DED animal models in general) is that the onset of desiccation is abrupt, as opposed to DED patients who typically suffer a progressive impairment of the tear film, which eventually elicits $CD4^+$ T cell-sustained ocular surface inflammation that aggravates the disease(92). Thus, ocular surface $CD4^+$ T cell activity may contribute indirectly to corneal epithelial damage during the initial phases of the disease in patients, as suggested by the faster tempo of corneal epitheliopathy in female WT mice (Supplementary Figure 1A). By contrast, the resistance of corneal nerves to experimental desiccation in the absence of $CD4^+$ T cells indicates that corneal neuropathy in DED is mostly immune-mediated. In line with this, we have previously shown that corneal nerves are particularly sensitive to the activation of Th1 $CD4^+$ T cells in the ocular surface in the absence of desiccating stress(43), and on the other hand, that signaling through transient receptor potential vanilloid-1 channels in the corneal tissue is required to propagate desiccation-initiated corneal nerve damage in DED(47). Therefore, it is likely that in the context of DED, sustained levels of Th1 cytokines from $CD4^+$ T cells prime corneal nerve changes that later propagate proximally through overactivation of transient receptor potential vanilloid-1 channels. More work is warranted in this direction since the mechanisms that promote corneal nerve alterations vary among ocular surface disorders(44). Nevertheless, our findings have implications for current DED management because they help explain why therapies aimed at reducing or controlling $CD4^+$ T cell recruitment and activation in the ocular surface may be more impactful on certain manifestations of the disease and not on others. At the same time, the present study also highlights the need for further research to elucidate the precise mechanisms underlying corneal epithelial and nerve damage in DED and to identify potential therapeutic targets for these conditions.

5. Data availability

The data underlying Figs. 3 and Supplementary Figures 3 and 4 are openly available in ArrayExpress (https://www.ebi.ac.uk/biostudies/arrayexpress), accession E-MTAB-13945.

6. Acknowledgments

Authors' contributions: AV, MP, MNG, AT, CDP, and JGG contributed to the conception and design of the work; AV, MP, AC, FS, IAK, DVA, AP, FF, CCV, MNG, and JGG contributed to the acquisition and analysis of data; AV, MP, MNG, AT, CDP, and JGG contributed to the interpretation of data; AV, MG, AT, MNG, CDP, and JGG drafted and/or substantively revised the manuscript. All authors read and approved the final manuscript.

Funding: This work was supported by research grants from Wellcome Trust (221859/Z/20/Z) and Agencia Nacional de Promoción Científica y Tecnológica (FONCyT PICT 2018-02911, PICT 2020-00138, PICT 2021-00109) awarded to JGG.

7. Bibliography

1. Galletti JG, Guzmán M, Giordano MN. Mucosal immune tolerance at the ocular surface in health and disease. Immunology. 2017 Apr;150(4):397–407.
2. Downie LE, Bandlitz S, Bergmanson JPG, Craig JP, Dutta D, Maldonado-Codina C, et al. CLEAR - Anatomy and physiology of the anterior eye. Cont Lens Anterior Eye. 2021 Apr;44(2):132–56.
3. Craig JP, Nichols KK, Akpek EK, Caffery B, Dua HS, Joo CK, et al. TFOS DEWS II Definition and Classification Report. Ocul Surf. 2017 Jul;15(3):276–83.
4. Tsubota K, Pflugfelder SC, Liu Z, Baudouin C, Kim HM, Messmer EM, et al. Defining Dry Eye from a Clinical Perspective. Int J Mol Sci. 2020 Dec 4;21(23):9271.
5. Galor A, Moein HR, Lee C, Rodriguez A, Felix ER, Sarantopoulos KD, et al. Review. Neuropathic Pain and Dry Eye. Ocul Surf. 2018 Jan;16(1):31–44.
6. Bron AJ, de Paiva CS, Chauhan SK, Bonini S, Gabison EE, Jain S, et al. TFOS DEWS II pathophysiology report. The Ocular Surface. 2017 Jul;15(3):438–510.
7. Periman LM, Perez VL, Saban DR, Lin MC, Neri P. The Immunological Basis of Dry Eye Disease and Current Topical Treatment Options. Journal of Ocular Pharmacology and Therapeutics. 2020 Apr 1;36(3):137–46.
8. Stevenson W, Chauhan SK, Dana R. Dry eye disease: an immune-mediated ocular surface disorder. Arch Ophthalmol. 2012 Jan;130(1):90–100.
9. Stern ME, Gao J, Schwalb TA, Ngo M, Tieu DD, Chan CC, et al. Conjunctival T-cell subpopulations in Sjögren's and non-Sjögren's patients with dry eye. Invest Ophthalmol Vis Sci. 2002 Aug;43(8):2609–14.
10. Jones L, Downie LE, Korb D, Benitez-Del-Castillo JM, Dana R, Deng SX, et al. TFOS DEWS II Management and Therapy Report. Ocul Surf. 2017 Jul;15(3):575–628.
11. Niederkorn JY, Stern ME, Pflugfelder SC, De Paiva CS, Corrales RM, Gao J, et al. Desiccating stress induces T cell-mediated Sjögren's Syndrome-like lacrimal keratoconjunctivitis. Journal of immunology (Baltimore, Md : 1950). 2006 Apr 1;176(7):3950–7.
12. De Paiva CS, Villarreal AL, Corrales RM, Rahman HT, Chang VY, Farley WJ, et al. Dry eye-induced conjunctival epithelial squamous metaplasia is modulated by interferon-gamma. Invest Ophthalmol Vis Sci. 2007 Jun;48(6):2553–60.
13. Schaumburg CS, Siemasko KF, De Paiva CS, Wheeler LA, Niederkorn JY, Pflugfelder SC, et al. Ocular surface APCs are necessary for autoreactive T cell-mediated experimental autoimmune lacrimal keratoconjunctivitis. J Immunol. 2011 Oct 1;187(7):3653–62.
14. El Annan J, Chauhan SK, Ecoiffier T, Zhang Q, Saban DR, Dana R. Characterization of effector T cells in dry eye disease. Invest Ophthalmol Vis Sci. 2009 Aug;50(8):3802–7.
15. Dohlman TH, Chauhan SK, Kodati S, Hua J, Chen Y, Omoto M, et al. The CCR6/CCL20 axis mediates Th17 cell migration to the ocular surface in dry eye disease. Invest Ophthalmol Vis Sci. 2013 Jun 12;54(6):4081–91.

16. Jackson DC, Zeng W, Wong CY, Mifsud EJ, Williamson NA, Ang CS, et al. Tear Interferon-Gamma as a Biomarker for Evaporative Dry Eye Disease. Invest Ophthalmol Vis Sci. 2016 Sep 1;57(11):4824–30.
17. Kumar NR, Praveen M, Narasimhan R, Khamar P, D'Souza S, Sinha-Roy A, et al. Tear biomarkers in dry eye disease: Progress in the last decade. Indian Journal of Ophthalmology. 2023 Apr;71(4):1190.
18. Pinto-Fraga J, Enríquez-de-Salamanca A, Calonge M, González-García MJ, López-Miguel A, López-de la Rosa A, et al. Severity, therapeutic, and activity tear biomarkers in dry eye disease: An analysis from a phase III clinical trial. Ocul Surf. 2018 Jul;16(3):368–76.
19. De Paiva CS, Chotikavanich S, Pangelinan SB, Pitcher JD, Fang B, Zheng X, et al. IL-17 disrupts corneal barrier following desiccating stress. Mucosal Immunol. 2009 May;2(3):243–53.
20. Chauhan SK, El Annan J, Ecoiffier T, Goyal S, Zhang Q, Saban DR, et al. Autoimmunity in dry eye is due to resistance of Th17 to Treg suppression. J Immunol. 2009 Feb 1;182(3):1247–52.
21. Coursey TG, Bian F, Zaheer M, Pflugfelder SC, Volpe EA, de Paiva CS. Age-related spontaneous lacrimal keratoconjunctivitis is accompanied by dysfunctional T regulatory cells. Mucosal Immunol. 2017 May;10(3):743–56.
22. Schaefer L, Trujillo-Vargas CM, Midani FS, Pflugfelder SC, Britton RA, de Paiva CS. Gut Microbiota From Sjögren syndrome Patients Causes Decreased T Regulatory Cells in the Lymphoid Organs and Desiccation-Induced Corneal Barrier Disruption in Mice. Front Med (Lausanne). 2022;9:852918.
23. Annunziato F, Romagnani C, Romagnani S. The 3 major types of innate and adaptive cell-mediated effector immunity. J Allergy Clin Immunol. 2015 Mar;135(3):626–35.
24. Hirahara K, Nakayama T. CD4+ T cell subsets in inflammatory diseases: beyond the Th1/Th2 paradigm. International Immunology. 2016 Apr 1;28(4):163–71.
25. Zhang X, Chen W, De Paiva CS, Corrales RM, Volpe EA, McClellan AJ, et al. Interferon-γ Exacerbates Dry Eye–Induced Apoptosis in Conjunctiva through Dual Apoptotic Pathways. Invest Ophthalmol Vis Sci. 2011 Aug;52(9):6279–85.
26. Zhang X, De Paiva CS, Su Z, Volpe EA, Li DQ, Pflugfelder SC. Topical interferon-gamma neutralization prevents conjunctival goblet cell loss in experimental murine dry eye. Exp Eye Res. 2014 Jan;118:117–24.
27. Zhang X, Chen W, De Paiva CS, Volpe EA, Gandhi NB, Farley WJ, et al. Desiccating stress induces CD4+ T-cell-mediated Sjögren's syndrome-like corneal epithelial apoptosis via activation of the extrinsic apoptotic pathway by interferon-γ. Am J Pathol. 2011 Oct;179(4):1807–14.
28. Yang X, Zuo X, Zeng H, Liao K, He D, Wang B, et al. IFN-γ Facilitates Corneal Epithelial Cell Pyroptosis Through the JAK2/STAT1 Pathway in Dry Eye. Invest Ophthalmol Vis Sci. 2023 Mar 29;64(3):34.
29. Ko JH, Kim S, Ryu JS, Song HJ, Oh JY. Interferon-γ elicits the ocular surface pathology mimicking dry eye through direct modulation of resident corneal cells. Cell Death Discov. 2023 Jun 30;9(1):209.
30. Zhang X, Volpe EA, Gandhi NB, Schaumburg CS, Siemasko KF, Pangelinan SB, et al. NK cells promote Th-17 mediated corneal barrier disruption in dry eye. PLoS One. 2012;7(5):e36822.
31. Chauhan SK, Jin Y, Goyal S, Lee HS, Fuchsluger TA, Lee HK, et al. A novel pro-lymphangiogenic function for Th17/IL-17. Blood. 2011 Oct 27;118(17):4630–4.
32. Ivashkiv LB. IFNγ: signalling, epigenetics and roles in immunity, metabolism, disease and cancer immunotherapy. Nat Rev Immunol. 2018 Sep;18(9):545–58.
33. Mills KHG. IL-17 and IL-17-producing cells in protection versus pathology. Nat Rev Immunol. 2023 Jan;23(1):38–54.
34. Chen Y, Chauhan SK, Saban DR, Sadrai Z, Okanobo A, Dana R. Interferon-γ-secreting NK cells promote induction of dry eye disease. J Leukoc Biol. 2011 Jun;89(6):965–72.
35. Coursey TG, Bohat R, Barbosa FL, Pflugfelder SC, de Paiva CS. Desiccating stress-induced chemokine expression in the epithelium is dependent on upregulation of NKG2D/RAE-1 and release of IFN-γ in experimental dry eye. J Immunol. 2014 Nov 15;193(10):5264–72.
36. Alam J, Yazdanpanah G, Ratnapriya R, Borcherding N, de Paiva CS, Li D, et al. IL-17 Producing Lymphocytes Cause Dry Eye and Corneal Disease With Aging in RXRα Mutant Mouse. Front Med (Lausanne). 2022;9:849990.
37. Alam J, Yazdanpanah G, Ratnapriya R, Borcherding N, de Paiva CS, Li D, et al. Single-cell

transcriptional profiling of murine conjunctival immune cells reveals distinct populations expressing homeostatic and regulatory genes. Mucosal Immunol. 2022 Apr;15(4):620–8.
38. Vereertbrugghen A, Galletti JG. Corneal nerves and their role in dry eye pathophysiology. Exp Eye Res. 2022 Jul 15;109191.
39. Guerrero-Moreno A, Baudouin C, Melik Parsadaniantz S, Réaux-Le Goazigo A. Morphological and Functional Changes of Corneal Nerves and Their Contribution to Peripheral and Central Sensory Abnormalities. Front Cell Neurosci. 2020;14:610342.
40. Stepp MA, Tadvalkar G, Hakh R, Pal-Ghosh S. Corneal epithelial cells function as surrogate Schwann cells for their sensory nerves. Glia. 2017 Jun;65(6):851–63.
41. Stepp MA, Pal-Ghosh S, Tadvalkar G, Williams A, Pflugfelder SC, de Paiva CS. Reduced intraepithelial corneal nerve density and sensitivity accompany desiccating stress and aging in C57BL/6 mice. Experimental Eye Research. 2018 Apr;169:91–8.
42. Guzmán M, Miglio M, Keitelman I, Shiromizu CM, Sabbione F, Fuentes F, et al. Transient tear hyperosmolarity disrupts the neuroimmune homeostasis of the ocular surface and facilitates dry eye onset. Immunology. 2020 Oct 14;161(2):148–61.
43. Vereertbrugghen A, Pizzano M, Sabbione F, Keitelman IA, Shiromizu CM, Aguilar DV, et al. An ocular Th1 immune response promotes corneal nerve damage independently of the development of corneal epitheliopathy. J Neuroinflammation. 2023 May 22;20(1):120.
44. Royer DJ, Echegaray-Mendez J, Lin L, Gmyrek GB, Mathew R, Saban DR, et al. Complement and CD4+ T cells drive context-specific corneal sensory neuropathy. Elife. 2019 Aug 15;8:e48378.
45. Stapleton F, Alves M, Bunya VY, Jalbert I, Lekhanont K, Malet F, et al. TFOS DEWS II Epidemiology Report. The ocular surface. 2017 Jul;15(3):334–65.
46. Mecum NE, Demers D, Sullivan CE, Denis TE, Kalliel JR, Meng ID. Lacrimal gland excision in male and female mice causes ocular pain and anxiety-like behaviors. Sci Rep [Internet]. 2020 Oct 14 [cited 2021 Jun 15];10. Available from: https://www.ncbi.nlm.nih.gov/pmc/articles/PMC7560880/
47. Pizzano M, Vereertbrugghen A, Cernutto A, Sabbione F, Keitelman IA, Shiromizu CM, et al. TRPV1 channels facilitate axonal degeneration of corneal sensory nerves in dry eye. Am J Pathol. 2024 Feb 5;S0002-9440(24)00047-6.
48. Yamazaki R, Yamazoe K, Yoshida S, Hatou S, Inagaki E, Okano H, et al. The Semaphorin 3A inhibitor SM-345431 preserves corneal nerve and epithelial integrity in a murine dry eye model. Sci Rep [Internet]. 2017 Nov 14 [cited 2021 Apr 20];7. Available from: https://www.ncbi.nlm.nih.gov/pmc/articles/PMC5686158/
49. Tadvalkar G, Pal-Ghosh S, Pajoohesh-Ganji A, Stepp MA. The impact of euthanasia and enucleation on mouse corneal epithelial axon density and nerve terminal morphology. Ocul Surf. 2020 Oct;18(4):821–8.
50. Yun H, Lathrop KL, St Leger AJ. A whole-mount immunohistochemistry protocol for detection of mouse corneal nerves. STAR Protoc. 2021 Sep 17;2(3):100734.
51. Guzmán M, Miglio M, Keitelman I, Shiromizu CM, Sabbione F, Fuentes F, et al. Transient tear hyperosmolarity disrupts the neuroimmune homeostasis of the ocular surface and facilitates dry eye onset. Immunology. 2020 Oct;161(2):148–61.
52. Katzenell S, Cabrera JR, North BJ, Leib DA. Isolation, Purification, and Culture of Primary Murine Sensory Neurons. Methods Mol Biol. 2017;1656:229–51.
53. Stevenson W, Chen Y, Lee SM, Lee HS, Hua J, Dohlman T, et al. Extraorbital lacrimal gland excision: a reproducible model of severe aqueous tear-deficient dry eye disease. Cornea. 2014 Dec;33(12):1336–41.
54. Guzmán M, Keitelman I, Sabbione F, Trevani AS, Giordano MN, Galletti JG. Mucosal tolerance disruption favors disease progression in an extraorbital lacrimal gland excision model of murine dry eye. Experimental eye research. 2016 Oct;151:19–22.
55. Yoon KC, Ahn KY, Choi W, Li Z, Choi JS, Lee SH, et al. Tear production and ocular surface changes in experimental dry eye after elimination of desiccating stress. Invest Ophthalmol Vis Sci. 2011 Sep 21;52(10):7267–73.
56. Chen Y, Chauhan SK, Lee HS, Saban DR, Dana R. Chronic dry eye disease is principally mediated by effector memory Th17 cells. Mucosal Immunol. 2014 Jan;7(1):38–45.
57. Murube J, Rivas L. Impression cytology on conjunctiva and cornea in dry eye patients establishes a correlation between squamous metaplasia and dry eye clinical severity. Eur J

Ophthalmol. 2003 Mar;13(2):115–27.
58. Pflugfelder SC, Tseng SC, Yoshino K, Monroy D, Felix C, Reis BL. Correlation of goblet cell density and mucosal epithelial membrane mucin expression with rose bengal staining in patients with ocular irritation. Ophthalmology. 1997 Feb;104(2):223–35.
59. Welss J, Punchago N, Feldt J, Paulsen F. The distribution of conjunctival goblet cells in mice. Ann Anat. 2021 Mar;234:151664.
60. Bron AJ, Argüeso P, Irkec M, Bright FV. Clinical staining of the ocular surface: mechanisms and interpretations. Prog Retin Eye Res. 2015 Jan;44:36–61.
61. Fabiani C, Barabino S, Rashid S, Dana MR. Corneal Epithelial Proliferation and Thickness in a Mouse Model of Dry Eye. Exp Eye Res. 2009 Aug;89(2):166–71.
62. Aczél T, Kun J, Szőke É, Rauch T, Junttila S, Gyenesei A, et al. Transcriptional Alterations in the Trigeminal Ganglia, Nucleus and Peripheral Blood Mononuclear Cells in a Rat Orofacial Pain Model. Frontiers in Molecular Neuroscience [Internet]. 2018 [cited 2024 Feb 19];11. Available from: https://www.ncbi.nlm.nih.gov/pmc/articles/PMC6028693/
63. Liu Q, Mai L, Yang S, Jia S, Chu Y, He H, et al. Transcriptional Alterations of Mouse Trigeminal Ganglion Neurons Following Orofacial Inflammation Revealed by Single-Cell Analysis. Front Cell Neurosci. 2022;16:885569.
64. Chung MK, Park J, Asgar J, Ro JY. Transcriptome analysis of trigeminal ganglia following masseter muscle inflammation in rats. Mol Pain. 2016 Oct 4;12:1744806916668526.
65. Katz HR, Arcese AA, Bloom O, Morgan JR. Activating Transcription Factor 3 (ATF3) is a Highly Conserved Pro-regenerative Transcription Factor in the Vertebrate Nervous System. Front Cell Dev Biol. 2022 Mar 8;10:824036.
66. Jessen KR, Mirsky R. The Success and Failure of the Schwann Cell Response to Nerve Injury. Front Cell Neurosci. 2019;13:33.
67. Ma CHE, Palmer A, Taylor JSH. Synergistic effects of osteonectin and NGF in promoting survival and neurite outgrowth of superior cervical ganglion neurons. Brain Res. 2009 Sep 15;1289:1–13.
68. Fu H, Fang P, Zhou HY, Zhou J, Yu XW, Ni M, et al. Acid-sensing ion channels in trigeminal ganglion neurons innervating the orofacial region contribute to orofacial inflammatory pain. Clin Exp Pharmacol Physiol. 2016 Feb;43(2):193–202.
69. Kim AY, Tang Z, Liu Q, Patel KN, Maag D, Geng Y, et al. Pirt, a Phosphoinositide-Binding Protein, Functions as a Regulatory Subunit of TRPV1. Cell. 2008 May 2;133(3):475–85.
70. Alles SRA, Smith PA. Peripheral Voltage-Gated Cation Channels in Neuropathic Pain and Their Potential as Therapeutic Targets. Front Pain Res (Lausanne). 2021 Dec 13;2:750583.
71. Mecklenburg J, Shein SA, Malmir M, Hovhannisyan AH, Weldon K, Zou Y, et al. Transcriptional profiles of non-neuronal and immune cells in mouse trigeminal ganglia. Front Pain Res (Lausanne). 2023 Oct 31;4:1274811.
72. Wack G, Metzner K, Kuth MS, Wang E, Bresnick A, Brandes RP, et al. Nox4-dependent upregulation of S100A4 after peripheral nerve injury modulates neuropathic pain processing. Free Radical Biology and Medicine. 2021 May 20;168:155–67.
73. Mao Q, Tian L, Wei J, Zhou X, Cheng H, Zhu X, et al. Transcriptome analysis of microRNAs, circRNAs, and mRNAs in the dorsal root ganglia of paclitaxel-induced mice with neuropathic pain. Front Mol Neurosci [Internet]. 2022 Aug 31 [cited 2024 Mar 15];15. Available from: https://www.frontiersin.org/articles/10.3389/fnmol.2022.990260
74. Pflugfelder SC, Corrales RM, de Paiva CS. T helper cytokines in dry eye disease. Exp Eye Res. 2013 Dec;117:118–25.
75. Foulsham W, Mittal SK, Taketani Y, Chen Y, Nakao T, Chauhan SK, et al. Aged Mice Exhibit Severe Exacerbations of Dry Eye Disease with an Amplified Memory Th17 Cell Response. Am J Pathol. 2020 Jul;190(7):1474–82.
76. Kodati S, Chauhan SK, Chen Y, Dohlman TH, Karimian P, Saban D, et al. CCR7 is critical for the induction and maintenance of Th17 immunity in dry eye disease. Invest Ophthalmol Vis Sci. 2014 Aug 19;55(9):5871–7.
77. Ji YW, Mittal SK, Hwang HS, Chang EJ, Lee JH, Seo Y, et al. Lacrimal gland-derived IL-22 regulates IL-17-mediated ocular mucosal inflammation. Mucosal Immunol. 2017 Sep;10(5):1202–10.
78. Chen Y, Chauhan SK, Shao C, Omoto M, Inomata T, Dana R. IFN-γ-Expressing Th17 Cells Are Required for Development of Severe Ocular Surface Autoimmunity. J Immunol. 2017 Aug

1;199(3):1163–9.
79. Lee OL, Tepelus TC, Huang J, Irvine AG, Irvine C, Chiu GB, et al. Evaluation of the corneal epithelium in non-Sjögren's and Sjögren's dry eyes: an in vivo confocal microscopy study using HRT III RCM. BMC Ophthalmol [Internet]. 2018 Dec 4 [cited 2021 Apr 19];18. Available from: https://www.ncbi.nlm.nih.gov/pmc/articles/PMC6278105/
80. Li F, Zhang Q, Ying X, He J, Jin Y, Xu H, et al. Corneal nerve structure in patients with primary Sjögren's syndrome in China. BMC Ophthalmol. 2021 May 12;21(1):211.
81. Bitirgen G, Kucuk A, Ergun MC, Satirtav G, Malik RA. Corneal nerve loss and increased Langerhans cells are associated with disease severity in patients with rheumatoid arthritis. Eye (Lond). 2023 Oct;37(14):2950–5.
82. Barros A, Queiruga-Piñeiro J, Lozano-Sanroma J, Alcalde I, Gallar J, Fernández-Vega Cueto L, et al. Small fiber neuropathy in the cornea of Covid-19 patients associated with the generation of ocular surface disease. Ocul Surf. 2022 Jan;23:40–8.
83. Pokhilko A, Nash A, Cader MZ. Common transcriptional signatures of neuropathic pain. Pain. 2020 Jul;161(7):1542–54.
84. Xu FF, Kong LC, Cao DL, Ding BX, Wu Q, Ding YC, et al. Decoding gene expression signatures in mice trigeminal ganglion across trigeminal neuropathic pain stages via high-throughput sequencing. Brain Res Bull. 2022 Sep;187:122–37.
85. Guimarães RM, Aníbal-Silva CE, Davoli-Ferreira M, Gomes FIF, Mendes A, Cavallini MCM, et al. Neuron-associated macrophage proliferation in the sensory ganglia is associated with peripheral nerve injury-induced neuropathic pain involving CX3CR1 signaling. Elife. 2023 May 31;12:e78515.
86. Downie LE, Zhang X, Wu M, Karunaratne S, Loi JK, Senthil K, et al. Redefining the human corneal immune compartment using dynamic intravital imaging. Proc Natl Acad Sci U S A. 2023 Aug;120(31):e2217795120.
87. Loi JK, Alexandre YO, Senthil K, Schienstock D, Sandford S, Devi S, et al. Corneal tissue-resident memory T cells form a unique immune compartment at the ocular surface. Cell Rep. 2022 May 24;39(8):110852.
88. I.Y. Hasan ZA. Dry eye syndrome risk factors: A systemic review. Saudi J Ophthalmol. 2022 Feb 18;35(2):131–9.
89. Gorimanipalli B, Khamar P, Sethu S, Shetty R. Hormones and dry eye disease. Indian J Ophthalmol. 2023 Apr;71(4):1276–84.
90. Gao Y, Min K, Zhang Y, Su J, Greenwood M, Gronert K. Female-Specific Downregulation of Tissue Polymorphonuclear Neutrophils Drives Impaired Regulatory T Cell and Amplified Effector T Cell Responses in Autoimmune Dry Eye Disease. J Immunol. 2015 Oct 1;195(7):3086–99.
91. Pham TL, Kakazu A, He J, Bazan HEP. Mouse strains and sexual divergence in corneal innervation and nerve regeneration. FASEB J. 2019 Mar;33(3):4598–609.
92. Perez. Inflammatory basis for dry eye disease flares. Experimental Eye Research. 2020;

8. Figures and legends

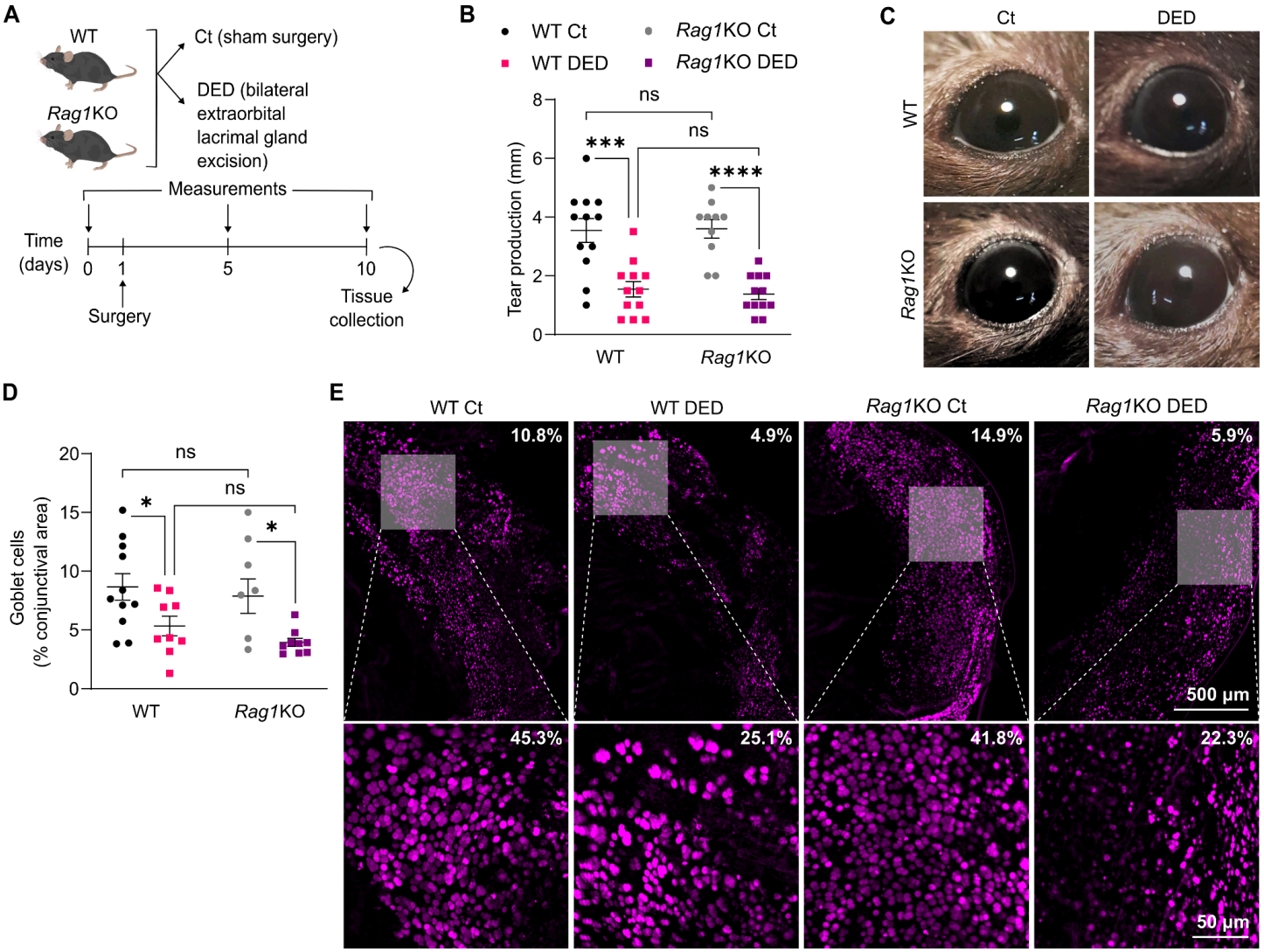

Figure 1 - Impact of adaptive immune deficiency on dry eye phenotype development. A) Dry eye disease (DED) was surgically induced in wild-type (WT) or recombination-activating gene 1-knockout (*Rag1*KO) mice of both sexes through bilateral excision of the extraorbital lacrimal gland. Sham-operated animals were included as controls (Ct). **B)** Tear production on day 5 as measured by phenol red-paper wetting length. **C)** External eye appearance of Ct and DED mice of both strains 10 days after surgery. **D)** Total conjunctival area occupied by goblet cells 10 days after DED induction. **E)** Representative micrographs of wheat germ agglutinin-stained goblet cells in conjunctival whole-mounts used for quantification. Low-magnification micrographs (top) of whole-mounted conjunctival strips used for measurements shown in D, with their corresponding high-magnification insets of the goblet cell-rich area (bottom) provided only as a reference. The actual goblet cell-occupied area is shown in the top right corner of each image. All experiments were performed twice or more with 6 mice/group/experiment. For all experiments, each data point represents one animal and the mean±standard error of measurement is shown. To compare means, two-way ANOVA was used for C and D (strain and treatment) with Sidak's post hoc test. * indicates $p<0.05$, *** indicates $p<0.001$, **** indicates $p<0.0001$, and ns indicates not significant.

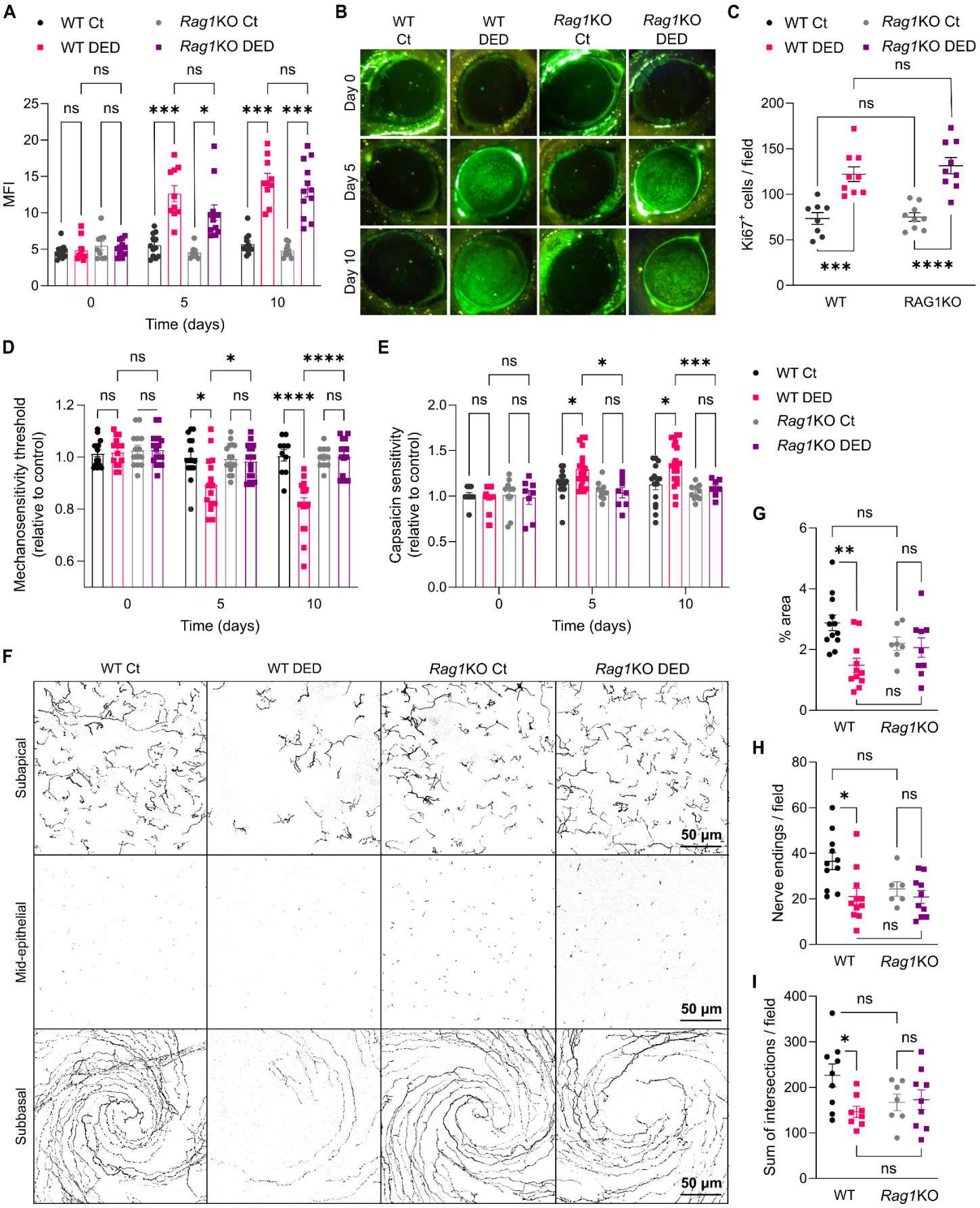
A
WT Ct
WT DED
Rag1KO Ct
Rag1KO DED
MFI
Time (days)
B
WT Ct
WT DED
Rag1KO Ct
Rag1KO DED
Day 0
Day 5
Day 10
C
Ki67+ cells / field
WT
RAG1KO
D
Mechanosensitivity threshold (relative to control)
Time (days)
E
Capsaicin sensitivity (relative to control)
Time (days)
F
Subapical
Mid-epithelial
Subbasal
50 µm
G
% area
H
Nerve endings / field
I
Sum of intersections / field

Figure 2 - Lack of adaptive immunity does not hinder corneal epitheliopathy but prevents corneal neuropathy development in dry eye. Dry eye disease (DED) was surgically induced in wild-type (WT) or recombination-activating gene 1-knockout (*Rag1*KO) mice of both sexes through bilateral excision of the extraorbital lacrimal gland. Sham-operated animals were included as controls (Ct). **A)** Cumulative data and **B)** representative micrographs of corneal dextran-fluorescein uptake in Ct and DED mice from both strains. Data shown as the mean fluorescence intensity (MFI) calculated with ImageJ software (Methods section). **C)** Number of proliferating (Ki67+) cells within the epithelial basal layer of corneal whole-mounts obtained 10 days after DED induction. **D)** Corneal mechanosensitivity and **E)** capsaicin thresholds in Ct and DED mice from both strains on days 0, 5, and 10 of DED induction. **F)** Representative micrographs and **G-H-I)** density of intraepithelial corneal innervation analyzed at three different levels by Alexa Fluor 488 anti-tubulin β3 staining: subapical (G, % area occupied by nerve endings) and mid-epithelial (H, count of nerve endings/field) nerve ending density and complexity of subbasal nerves (I, sum of intersections at all Sholl radii). All experiments were performed twice or more with 6 mice/group/experiment. For all experiments, each data point represents one animal and mean±standard error of measurement is shown. To compare means, two-way ANOVA was used for A, D, and E (group and time) and C, G, H, and I (strain and treatment) with Sidak's post hoc test. * indicates $p<0.05$, *** indicates $p<0.001$, **** indicates $p<0.0001$, and ns indicates not significant.

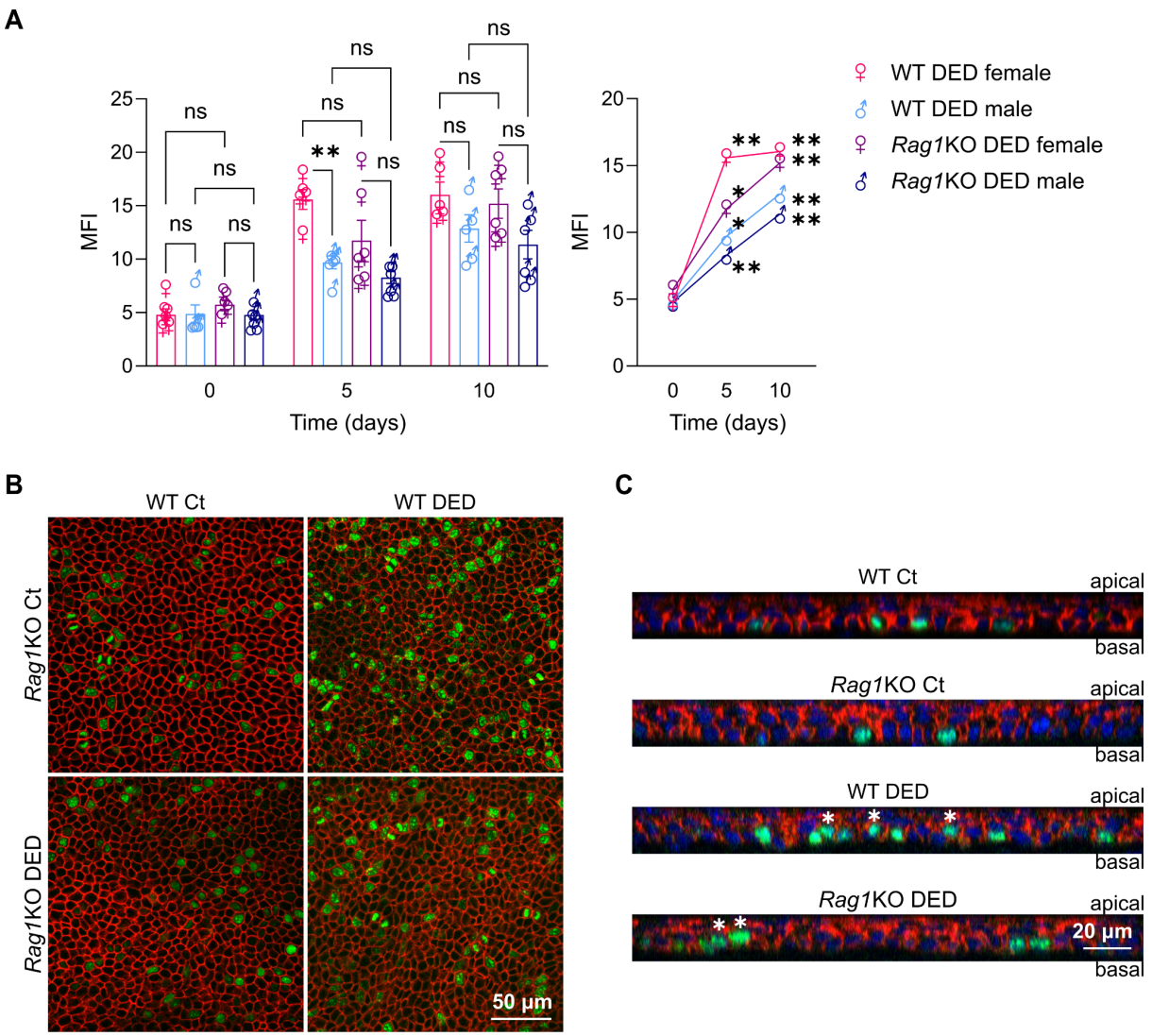

Supplementary Figure 1 - Effect of sex and epithelial cell turnover in dry eye-induced corneal epitheliopathy progression. Dry eye disease (DED) was surgically induced in wild-type (WT) or recombination-activating gene 1-knockout (*Rag1*KO) mice of both sexes through bilateral excision of the extraorbital lacrimal gland. **A)** Corneal dextran-fluorescein uptake in both strains was quantified as mean fluorescence intensity (MFI) calculated with ImageJ software (Methods section). Individual data (left) and progression curves (right) from two independent experiments. **B)** Representative micrographs of proliferating cells within the basal layer and **C)** axial reconstructions of the entire epithelium of corneal whole-mounts obtained 10 days after DED induction and stained with Ki67 (green) and E-cadherin (red). Nuclei are shown in blue whereas suprabasal Ki67+ epithelial cells are marked with white asterisks in the axial reconstructions. For all experiments, each data point represents one animal and mean±standard error of measurement is shown. To compare means, three-way ANOVA was used (strain, sex, and time) with Sidak's post hoc test. ♀ and ♂ indicate female and male, respectively; * indicates $p<0.05$, ** indicates $p<0.01$, and ns indicates not significant.

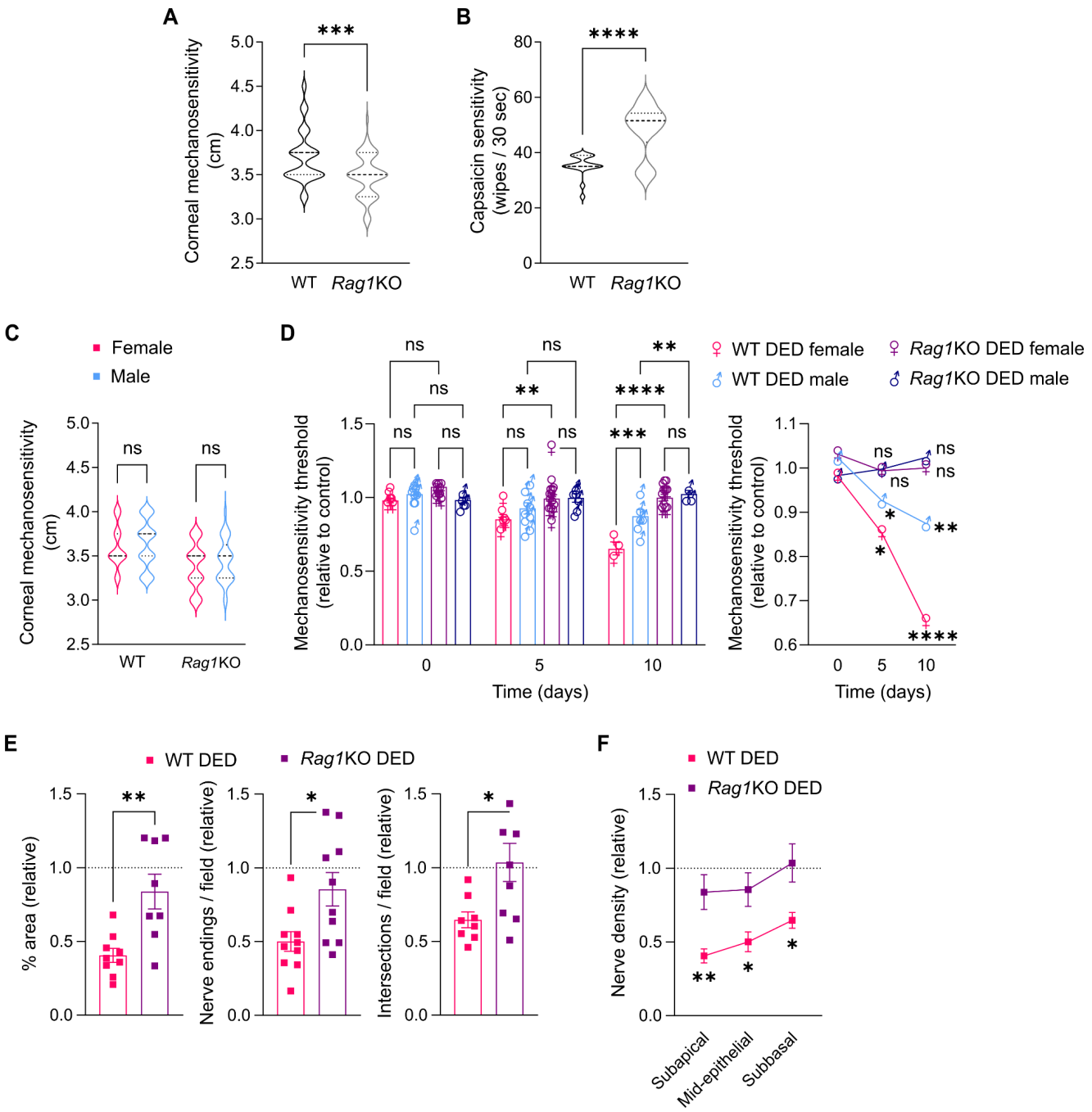

Supplementary Figure 2 - Strain-specific baseline differences and effect of sex and relative change in nerve density in dry eye-induced corneal neuropathy. Dry eye disease (DED) was surgically induced in wild-type (WT) or recombination-activating gene 1-knockout (*Rag1*KO) mice of both sexes through bilateral excision of the extraorbital lacrimal gland. Corneal mechanosensitivity and capsaicin sensitivity were measured using nylon 6-0 filaments or 100 μM capsaicin instillation during the experiment whereas nerve morphology was assessed by confocal microscopy and quantified as described in Methods. **A)** Baseline mechanosensitivity thresholds (pooled data) from 39 WT and 56 *Rag1*KO mice. **B)** Baseline capsaicin sensitivity thresholds (pooled data) from 34 WT and 18 *Rag1*KO mice. **C)** Baseline mechanosensitivity thresholds (pooled data) aggregated by sex from 53 WT (22 female and 31 male) and 48 *Rag1*KO mice (19 female and 29 male). **D)** Mechanosensitivity thresholds in female and male DED mice from both

strains on days 0, 5, and 10 of DED induction. Individual data (left) and progression curves (right) from two independent experiments. **E)** Change in nerve density in DED mice (females and males combined) from both strains shown relative to Ct mice of the same strain as analyzed at three different levels of intraepithelial corneal innervation: subapical endings (left), mid-epithelial fibers (middle), and subbasal nerves (right). **F)** Distribution of change in nerve density in DED mice (relative to Ct mice of the same strain, both sexes combined) over the three levels of intraepithelial corneal innervation. For all experiments, each data point represents one animal and mean±standard error of measurement is shown. To compare means, three-way ANOVA was used (strain, sex, and time) with Sidak's post hoc test. ♀ and ♂ indicate female and male, respectively; * indicates $p<0.05$, ** indicates $p<0.01$, and ns indicates not significant.

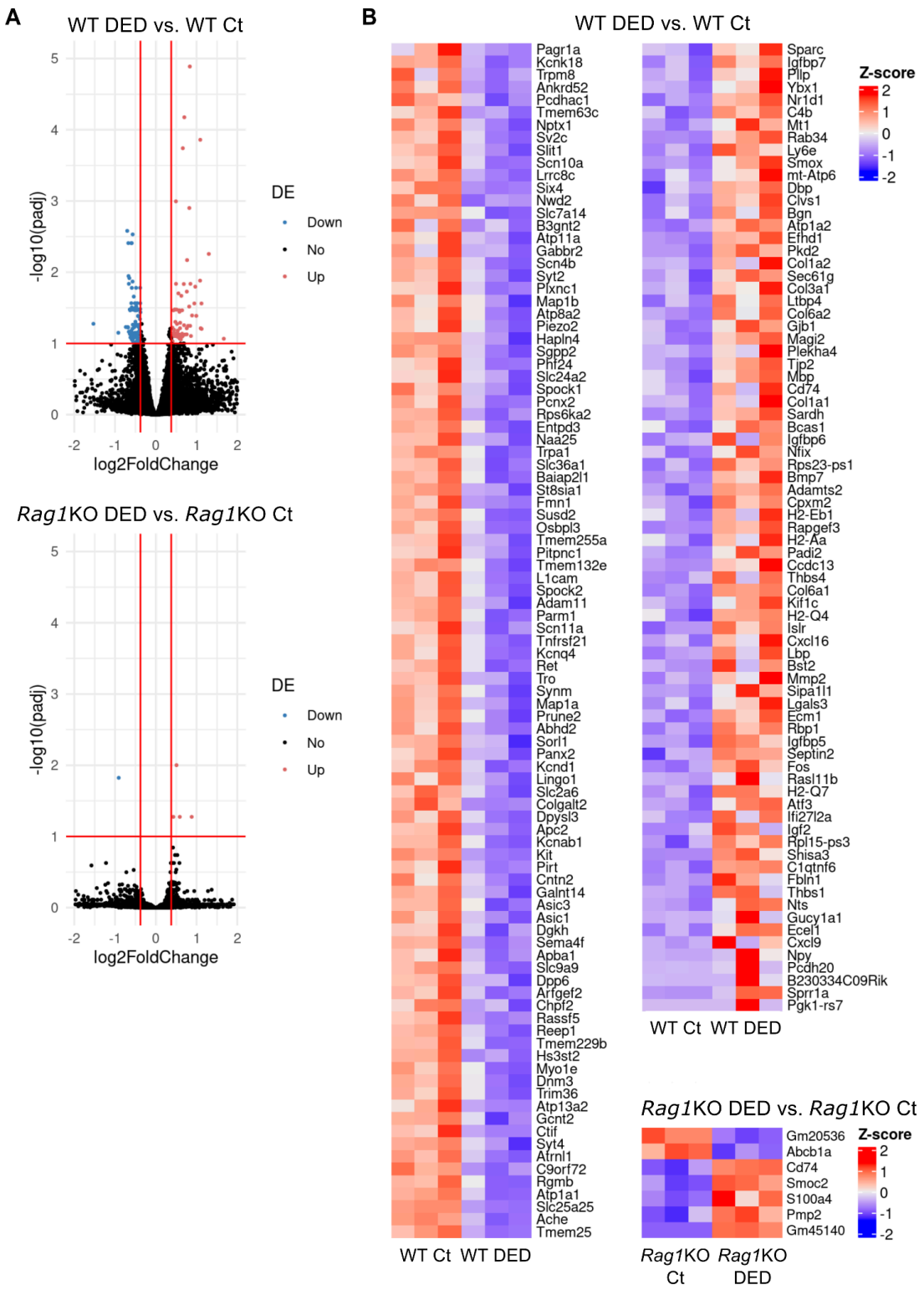

Figure 3 - Gene expression changes induced by dry eye disease in the trigeminal ganglion. Dry eye disease (DED) was surgically induced in wild-type (WT) or recombination-activating gene 1-knockout (*Rag1*KO) mice for 10 days and then the trigeminal ganglia were harvested for bulk RNA-Seq analysis (female mice, n=3 per group). Differential gene expression was calculated between the sham-operated (Ct) and DED mice of each strain. **A)** Volcano plots of differentially expressed genes in DED vs Ct mice of each strain. Up-regulated genes in DED mice are shown in red and down-regulated genes are shown in blue. **B)** Heatmaps (normalized counts, Z score) of

the differentially expressed genes (fold change > 1.3, adjusted p-value < 0.1) in Ct vs DED WT and *Rag1*KO mice.

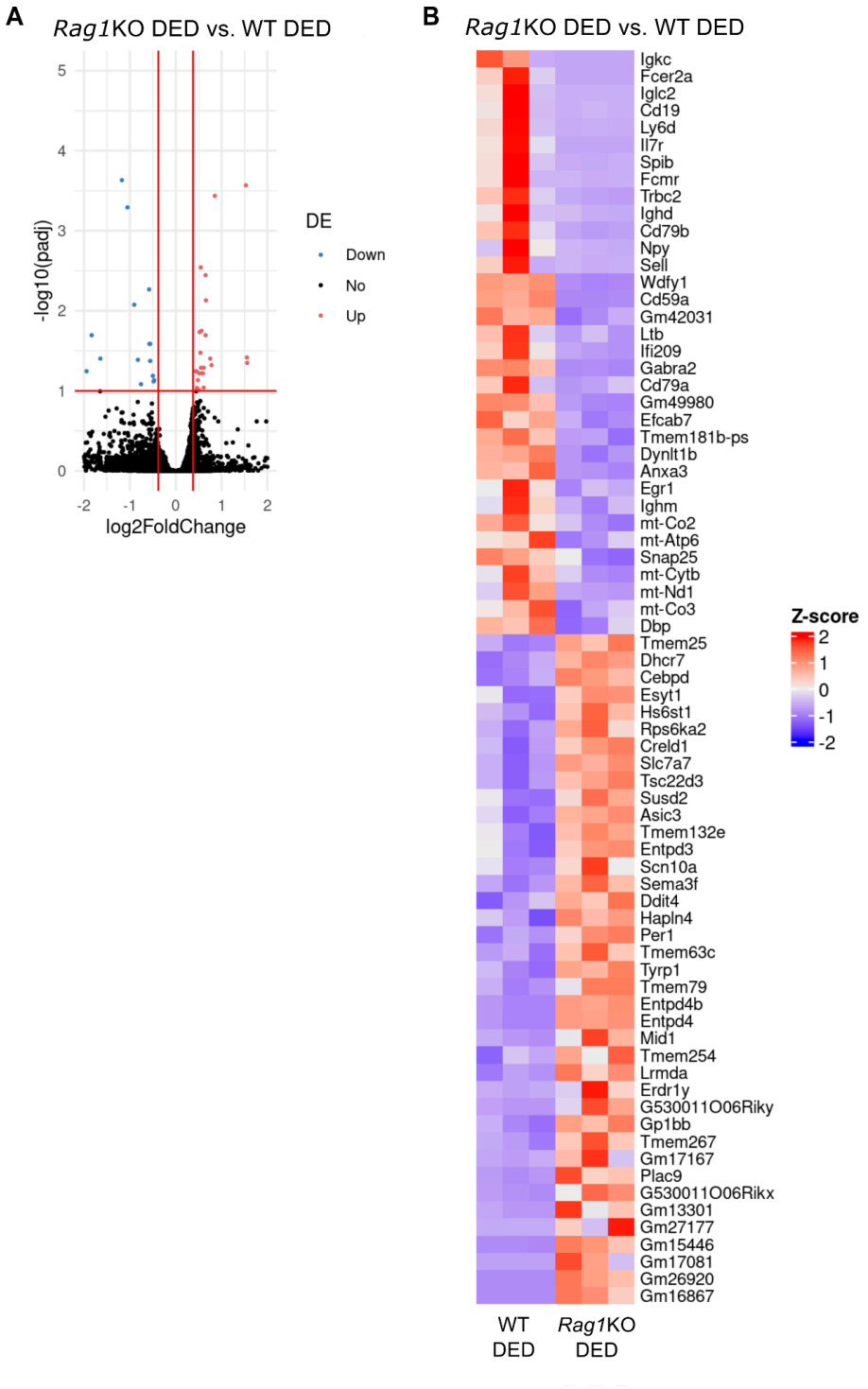

Supplementary Figure 3 - Comparison of dry eye-induced transcriptomic signatures in the trigeminal ganglion of wild-type and adaptive immune-deficient mice. Dry eye disease (DED) was surgically induced in wild-type (WT) or recombination-activating gene 1-knockout (*Rag1*KO) mice for 10 days and then the trigeminal ganglia were harvested for bulk RNA-Seq analysis (female mice, n=3 per group). Differential gene expression was calculated between the sham-operated (Ct) and DED mice of each strain. **A)** Volcano plots of differentially expressed genes in DED *Rag1*KO vs WT mice. Up-regulated genes in DED *Rag1*KO mice are shown in red

and down-regulated genes are shown in blue. **B)** Heatmaps (normalized counts, Z score) of the differentially expressed genes (fold change > 1.3, adjusted p-value < 0.1) in DED *Rag1*KO vs WT mice.

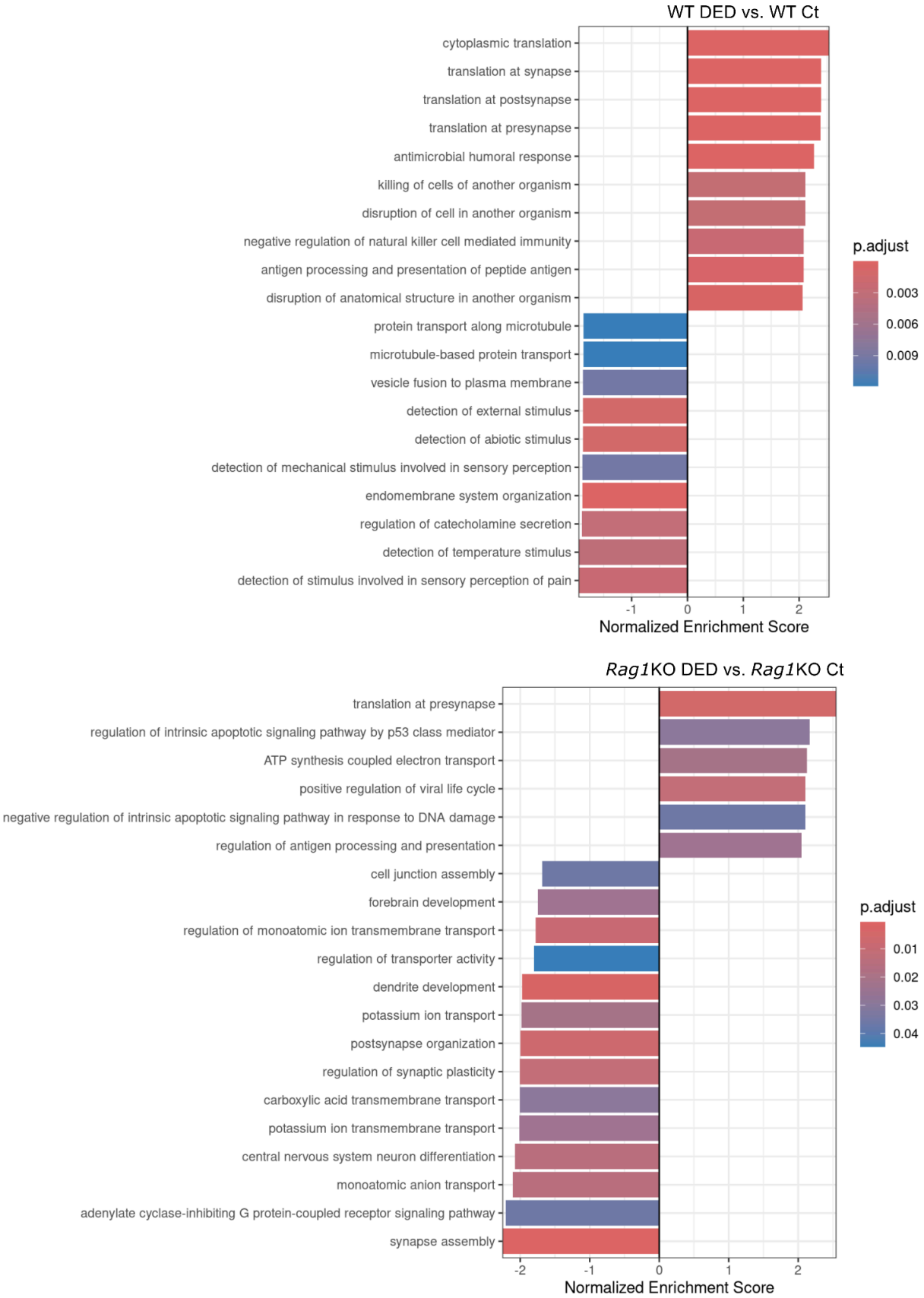

Supplementary Figure 4 - Biological pathways enriched in the dry eye-induced transcriptomic signatures in the trigeminal ganglion of wild-type and adaptive immune-deficient mice. Dry eye disease (DED) was surgically induced in wild-type (WT) or recombination-activating gene 1-knockout (*Rag1*KO) mice for 10 days and then the trigeminal ganglia were harvested for bulk RNA-Seq analysis (female mice, n=3 per group). Differential gene expression was calculated between the sham-operated (Ct) and DED mice of each strain, and then gene set enrichment analysis (Gene Ontology). The 10 most significantly activated and suppressed pathways for each strain are shown.

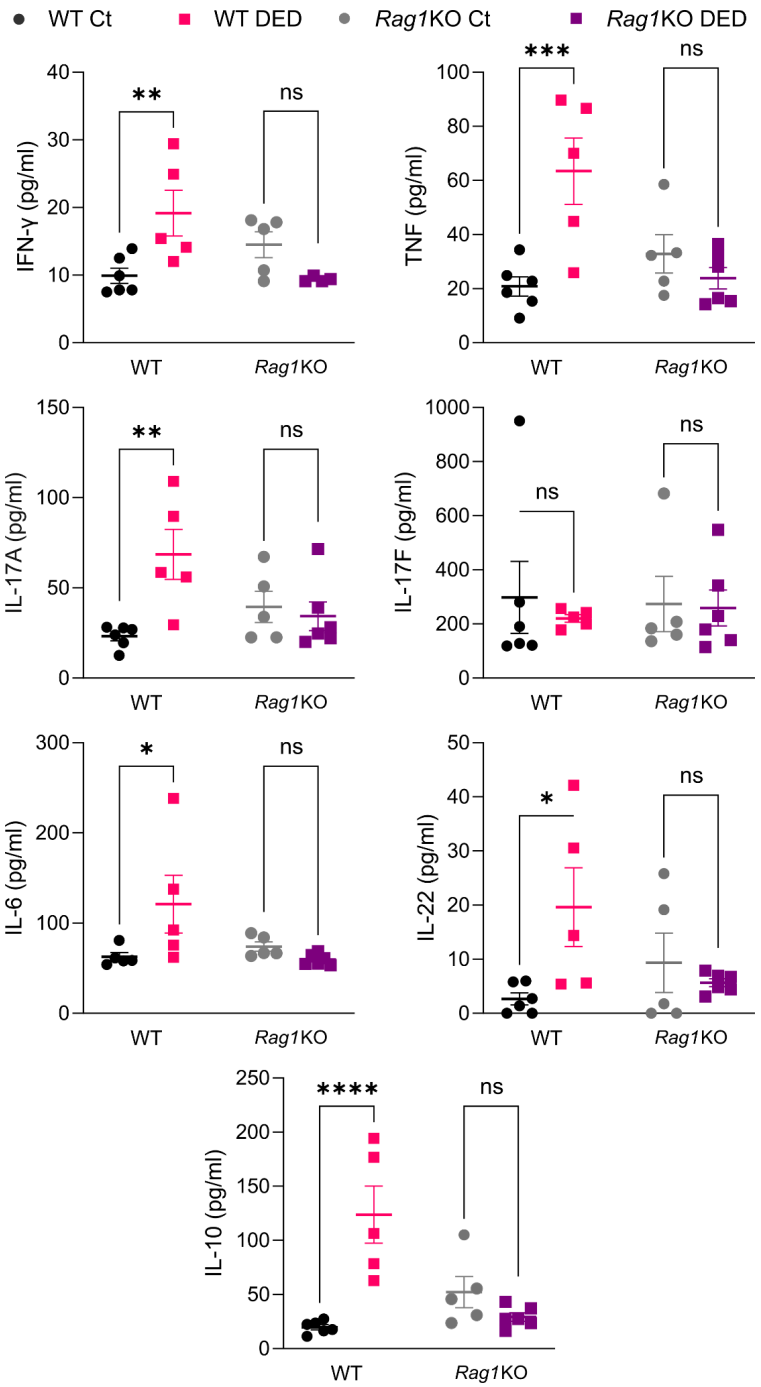

Figure 4 - Cytokine levels in tear washings of wild-type and T cell-deficient mice with dry eye. Tear washings were collected after 10 days of dry eye disease (DED) induction in wild-type (WT) or recombination-activating gene 1-knockout (Rag1KO) mice of both sexes and analyzed by a bead-based multiplex assay for interferon (IFN)-γ, tumor necrosis factor (TNF), interleukin (IL)-6, -10, -17A, -17F, and -22 levels. Results from one representative experiment with 6 mice/group are shown in pg/ml (mean±SEM). Two-way ANOVA (treatment and strain) with Sidak's post hoc test was used to compare means. * indicates $p<0.05$, ** indicates $p<0.01$, *** indicates $p<0.001$, **** indicates $p<0.0001$, and ns indicates not significant.

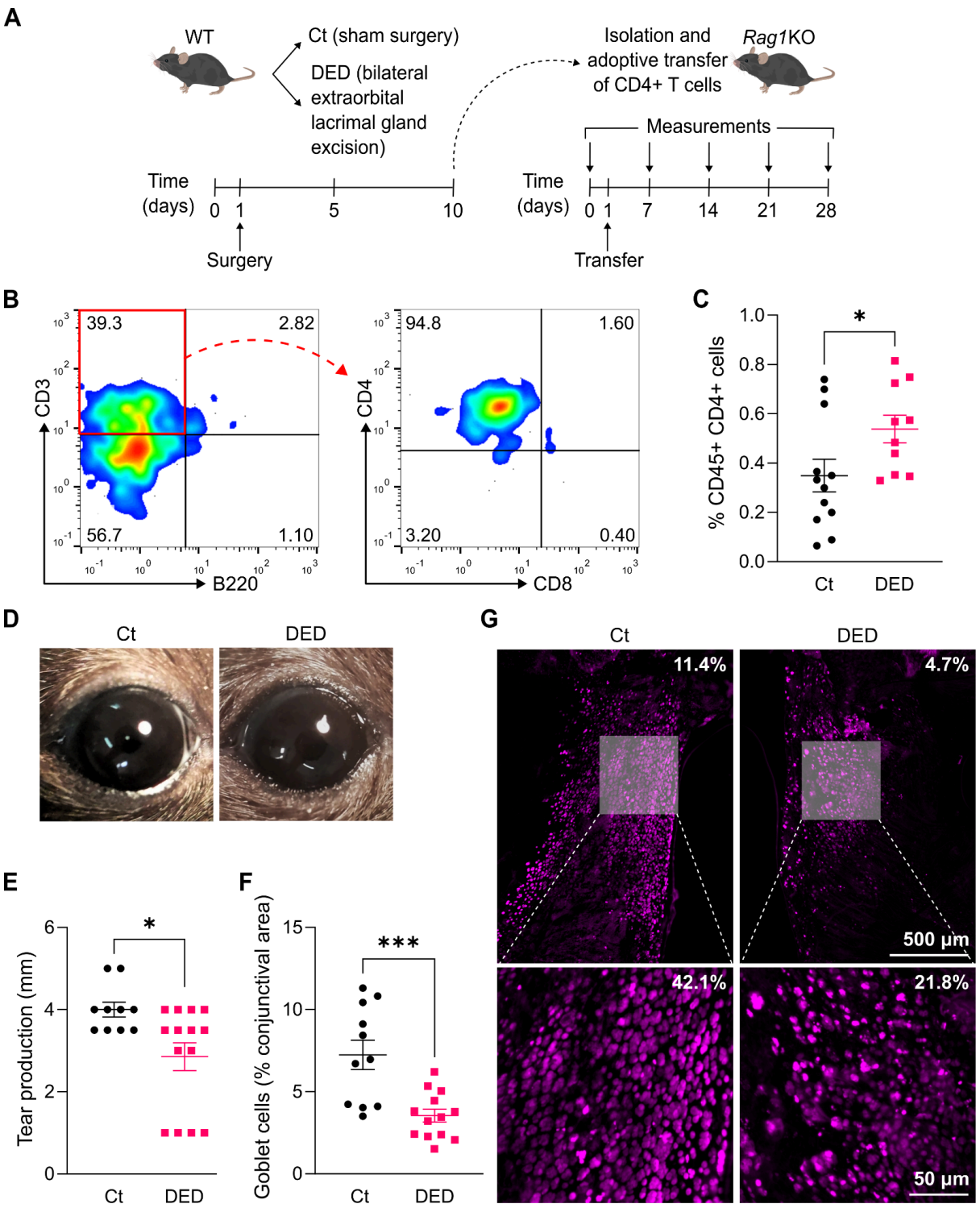

Figure 5 - Adoptive transfer of dry eye-induced CD4⁺ T cells reproduces ocular surface phenotype. A) Experimental design: CD4⁺ T cells were isolated from the spleens and lymph nodes of wild-type (WT) mice of both sexes 10 days after surgical induction of dry eye disease (DED) and then adoptively transferred into sex-matched recombination-activating gene 1-knockout (*Rag1*KO) mice, which were evaluated over the course of 4 weeks. Sham-operated WT mice were used as a source of control (Ct) CD4⁺ T cells. **B)** Flow cytometry of cervical lymph node cells (representative example) obtained from a CD4⁺ T cell-reconstituted *Rag1*KO mouse 4 weeks after transfer. **C)** Conjunctival CD4⁺ T cells in *Rag1*KO mice 4 weeks after transfer as assessed by flow cytometry

(gated on total viable cells). **D)** External eye appearance (representative micrographs) of *Rag1*KO recipients of Ct and DED-induced $CD4^+$ T cells in *Rag1*KO mice 4 weeks after transfer. **E)** Tear production in Ct- and DED-induced $CD4^+$ T cell recipients measured on days 25-27 after transfer. **F)** Total conjunctival area occupied by goblet cells in Ct- and DED-induced $CD4^+$ T cell recipients 4 weeks after transfer. **G)** Representative micrographs of wheat germ agglutinin-stained goblet cells in conjunctival whole-mounts used for quantification. Low-magnification micrographs (top) of whole-mounted conjunctival strips used for measurements shown in F, with their corresponding high-magnification insets of the goblet cell-rich area (bottom) provided only as a reference. The actual goblet cell-occupied area is shown in the top right corner of each image. All experiments were performed twice or more with 6 mice/group/experiment. For all experiments, mean±standard error of measurement is shown and each data point represents one animal. Student's t test was used to compare means. * indicates $p<0.05$ and *** indicates $p<0.001$.

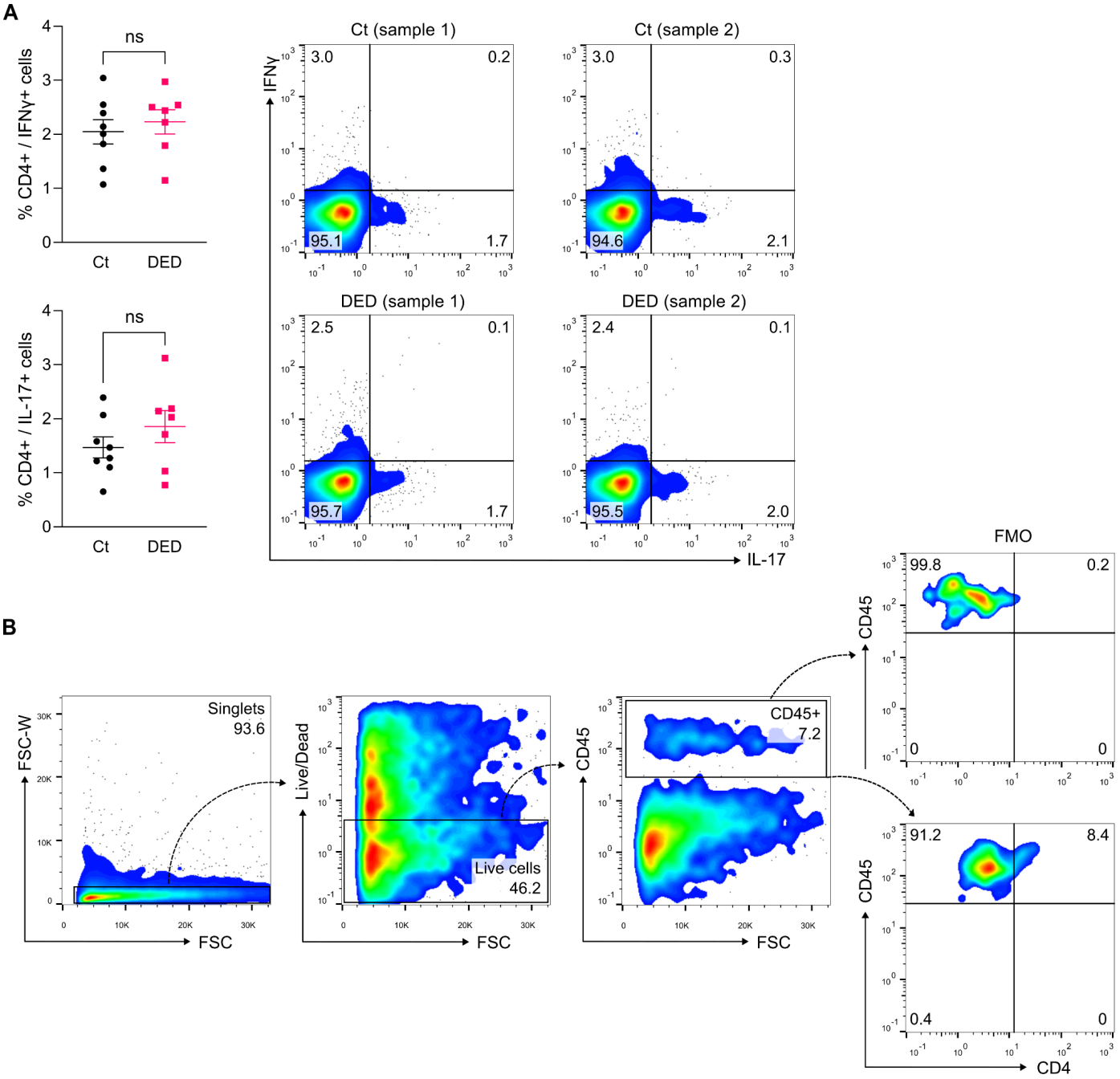

Supplementary Figure 5 - Adoptive transfer of dry eye-induced CD4⁺ T cells reproduces corneal neuropathy but not epitheliopathy. The experimental design was described in detail in Figure 5A and involved the adoptive transfer of control (Ct) or dry eye disease (DED)-induced CD4⁺ T cells from WT mice into recombination-activating gene 1-knockout (*Rag1*KO) mice of the same sex that were subsequently evaluated over 4 weeks. **A)** Production of interferon (IFN)-γ and interleukin (IL)-17 by Ct or DED-induced CD4⁺ T cells from WT mice after 10 days of induction as assessed by intracellular flow cytometry before the adoptive transfer into *Rag1*KO mice. Data from one experiment (left panel, n=7-8/group) and representative dot plots (right panel, 2 samples from each group). **B)** Gating strategy with representative example of flow cytometry analysis of conjunctival CD4⁺ T cells in *Rag1*KO mice 4 weeks after adoptive transfer. For A, mean±standard error of measurement is shown, each data point represents one animal, and Student's t test was

applied to compared means. FSC indicates forward side, FSC-W indicates forward scatter width, FMO indicates fluorescence-minus-one control, and ns indicates not significant.

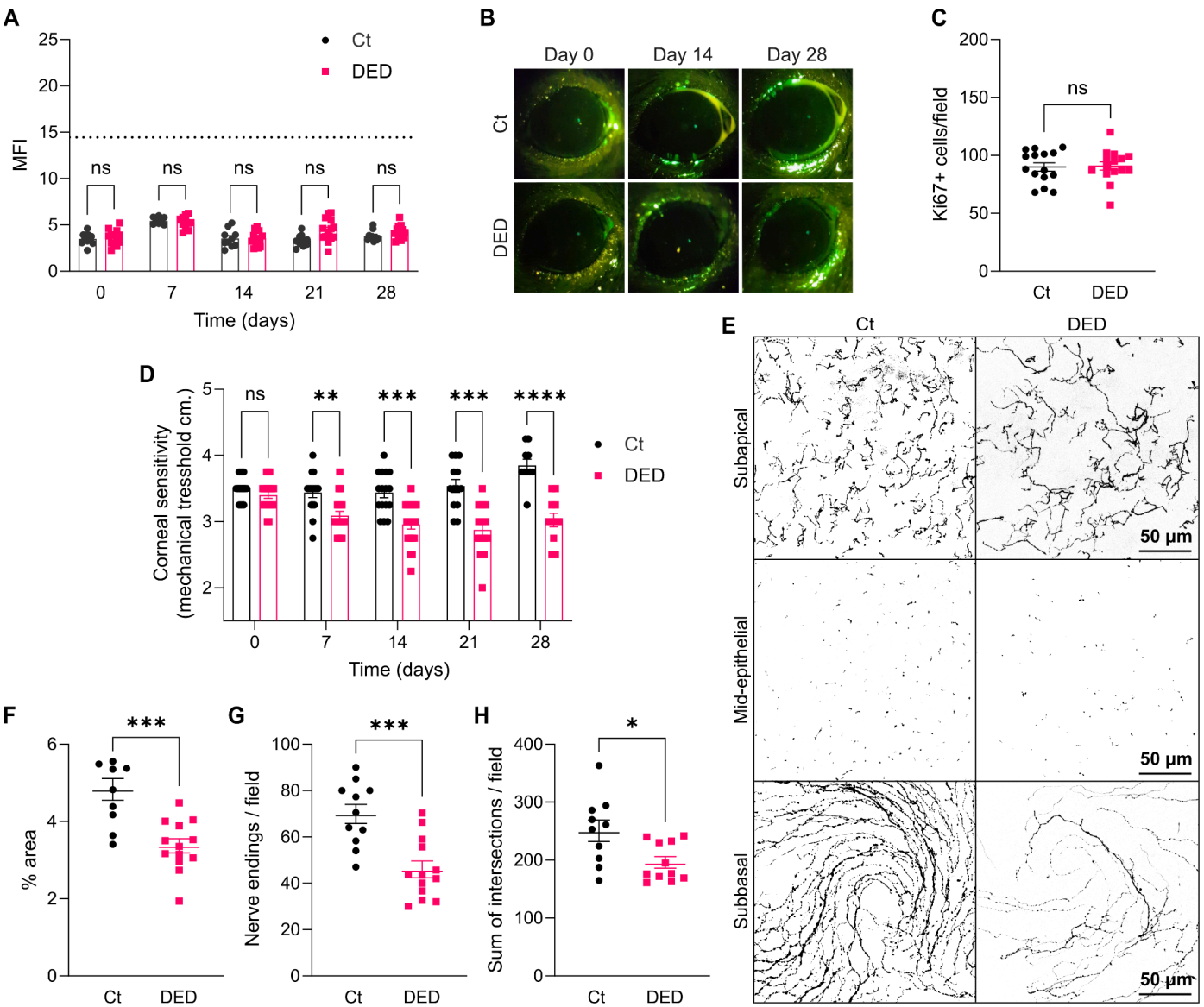

Figure 6 - Adoptive transfer of dry eye-induced CD4⁺ T cells reproduces corneal neuropathy but not epitheliopathy. The experimental design was described in detail in Figure 5A and involved the adoptive transfer of control (Ct) or dry eye disease (DED)-induced CD4⁺ T cells from WT mice into recombination-activating gene 1-knockout (*Rag1*KO) mice of the same sex that were subsequently evaluated over 4 weeks. **A)** Cumulative and **B)** representative micrographs of corneal dextran-fluorescein uptake in Ct- and DED-induced CD4⁺ T cell recipients. Data shown as the mean fluorescence intensity (MFI) calculated with ImageJ software (Methods section). The dotted line represents the mean corneal uptake observed in DED WT mice. **C)** Quantification of proliferating cells within the epithelial basal layer of corneal whole-mounts obtained from Ct- and DED-induced CD4⁺ T cell-recipient mice. **D)** Corneal mechanosensitivity thresholds in Ct- and DED-induced CD4⁺ T cell recipients. **E)** Representative micrographs and **F-H)** density of intraepithelial corneal innervation analyzed at three different levels by Alexa Fluor 488 anti-tubulin β3 staining: subapical (F, % area occupied by nerve endings) and mid-epithelial (G, count of nerve endings/field) nerve ending density and complexity of subbasal nerves (H, sum of intersections at all Sholl radii). All experiments were performed twice or more with 6 mice/group/experiment. For all

experiments, mean±standard error of measurement is shown and each data point represents one animal. To compare means, two-way ANOVA (donor group and time) with Sidak's post hoc test was used for A and D, and Student's t test was applied in C, F, G, and H. * indicates p<0.05, ** indicates p<0.01, *** indicates p<0.001, **** indicates p<0.0001, and ns indicates not significant.

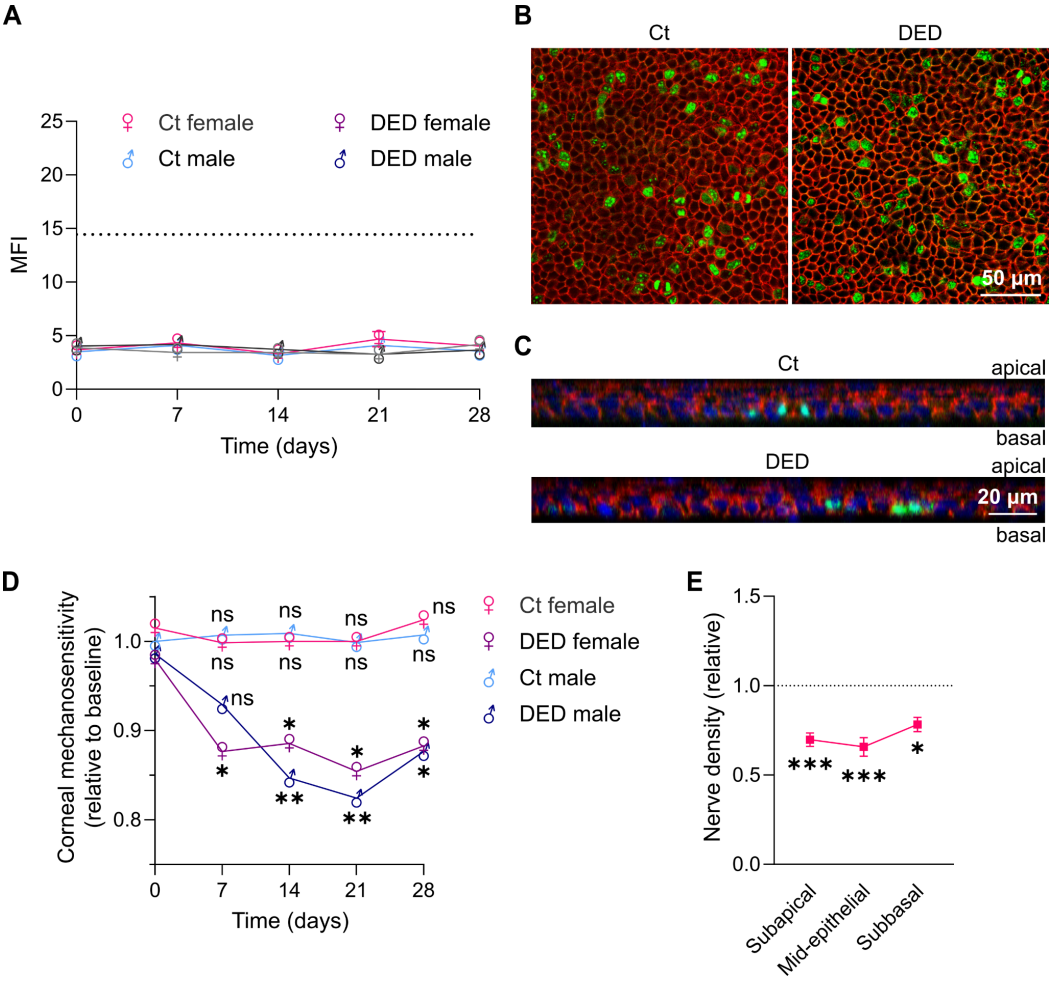

Supplementary Figure 6 - Adoptive transfer of dry eye-induced CD4⁺ T cells reproduces corneal neuropathy but not epitheliopathy. The experimental design was described in detail in Figure 5A and involved the adoptive transfer of control (Ct) or dry eye disease (DED)-induced CD4⁺ T cells from WT mice into recombination-activating gene 1-knockout (*Rag1*KO) mice of the same sex that were subsequently evaluated over 4 weeks. **A)** Sex-aggregated data of corneal dextran-fluorescein uptake in Ct- and DED-induced CD4⁺ T cell recipients. Data shown as the mean fluorescence intensity (MFI) calculated with ImageJ software (Methods section). **B)** Representative micrographs of proliferating cells within the basal layer and **C)** axial reconstructions of the entire epithelium of corneal whole-mounts obtained 4 weeks after adoptive transfer induction and stained with Ki67 (green) and E-cadherin (red). Nuclei are shown in blue in the axial reconstructions. **C)** Quantification of proliferating cells within the epithelial basal layer of corneal whole-mounts obtained from Ct- and DED-induced CD4⁺ T cell-recipient mice and stained with Ki67 (green) and E-cadherin (red). **D)** Corneal mechanosensitivity thresholds in Ct- and DED-induced CD4⁺ T cell recipients aggregated by sex. **E)** Distribution of change in nerve density over the three levels of intraepithelial corneal innervation in DED-induced CD4⁺ T cell-recipients

(both sexes combined, expressed relative to Ct $CD4^+$ T cell recipients). All experiments were performed twice or more with 6 mice/group/experiment. For all experiments, mean±standard error of measurement is shown and each data point represents one animal. To compare means, three-way ANOVA was used (strain, sex, and time) with Sidak's post hoc test was used for A and D, and Student's t test was applied in E. ♀ and ♂ indicate female and male, respectively; * indicates $p<0.05$, ** indicates $p<0.01$, *** indicates $p<0.001$, and ns indicates not significant.

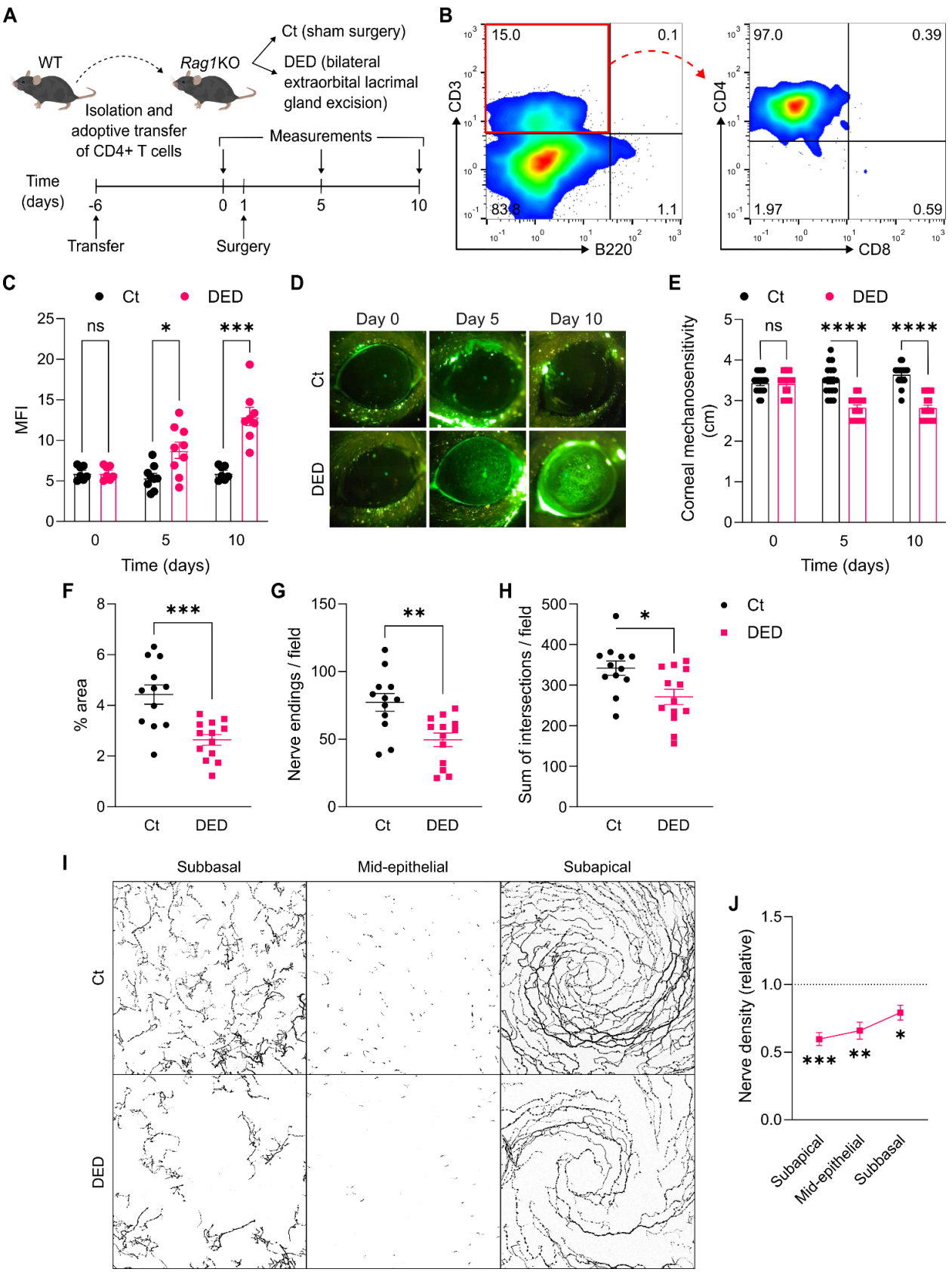

Figure 7 - Reconstitution of T cell-deficient with CD4⁺ T cells enables corneal neuropathy development upon dry eye induction. A) Experimental design: CD4⁺ T cells were isolated from the spleens and lymph nodes of wild-type (WT) mice of both sexes and then adoptively transferred into sex-matched recombination-activating gene 1-knockout (*Rag1*KO) mice, which one week later underwent either sham (Ct) or dry eye disease (DED)-inducing surgery and were evaluated over

the course of 10 days. **B)** Flow cytometry of cervical lymph node cells (representative example) obtained from a $CD4^+$ T cell-reconstituted *Rag1*KO mouse 10 days after surgery. **C)** Cumulative and **D)** representative micrographs of corneal dextran-fluorescein uptake in Ct and DED $CD4^+$ T cell-reconstituted *Rag1*KO mice. Data shown as the mean fluorescence intensity (MFI) calculated with ImageJ software (Methods section). **E)** Corneal mechanosensitivity thresholds in Ct and DED $CD4^+$ T cell-reconstituted *Rag1*KO mice. **F-H)** Quantification and **I)** representative micrographs of intraepithelial corneal innervation analyzed at three different levels by Alexa Fluor 488 anti-tubulin β3 staining: subapical (F, % area occupied by nerve endings) and mid-epithelial (G, count of nerve endings/field) nerve ending density and complexity of subbasal nerves (H, sum of intersections at all Sholl radii). **J)** Distribution of change in nerve density over the three levels of intraepithelial corneal innervation in DED $CD4^+$ T cell-reconstituted *Rag1*KO mice (expressed relative to Ct $CD4^+$ T cell-reconstituted mice). All experiments were performed twice or more with 6 mice/group/experiment. For all experiments, mean±standard error of measurement is shown and each data point represents one animal. To compare means, two-way ANOVA with Sidak's post hoc test was used in C and E (treatment and time), and Student's t test was applied in F, G, H, and J. * indicates $p<0.05$, ** indicates $p<0.01$, *** indicates $p<0.001$, **** indicates $p<0.0001$, and ns indicates not significant.